Geometrically Adaptive Milling of

Fan Blade Assembly Weld Fillets

GEOMETRICALLY ADAPTIVE MILLING OF FAN BLADE ASSEMBLY WELD FILLETS

BY

YU PIN LIN, B.ENG.MGMT.

A Thesis

Submitted to the School of Graduate Studies

in Partial Fulfilment of the Requirements

for the Degree

Master of Applied Science

McMaster University

MASTER OF APPLIED SCIENCE (2012) McMaster University

(Mechanical Engineering) Hamilton, Ontario, Canada

TITLE: Geometrically Adaptive Milling of Fan Blade Assembly Weld Fillets

AUTHOR: Yu Pin Lin

B.Eng.Mgmt., (Mechanical Engineering and Management)

McMaster University, Hamilton, Ontario, Canada

SUPERVISOR: Dr. Allan D. Spence

NUMBER OF PAGES: xv, 94

Abstract

Modern aeroengine design focuses on reducing overall weight and improving component service life. For fan blade assemblies, the blades and hub/shaft are attached by the most common dovetail (or fir tree) attachment design, which experiences fretting fatigue at the joint resulting in lower reliability and higher repair difficulty. A new joining design that connects blade /disk by welding and eliminates the attachment, has been implemented in military and commercial aeroengines. This joining design is most suitable for large diameter fan blades where single piece machining is impractical and time consuming. The joined blade requires post-process machining to remove excess weld material. However, because of varying assembly geometry, joints must be individually measured and tool paths consequently adjusted to match actual surface locations. The objective of this thesis is to develop an automated and geometrically adaptive post-process weld machining system.

This thesis proposes a solution that integrates surface digitization, computer aided design (CAD) and computer aided manufacturing (CAM) systems, to accommodate the part-to-part variation issue. The integrated system includes precise laser digitizing, geometric modelling, tool path customizing, coordinate registration and CNC machining. The core algorithm was designed on the open and object-oriented C++ ACIS/HOOPS

kernel. The customized tool paths are prepared based on the misalignment distance measured by laser digitizing, and a custom developed mathematical correction algorithm that can be implemented on a typical personal computer. At present, the machining process is designed for a three-axis machine tool. Suggested future works include implementation on a five-axis machine, and feed rate optimized tool paths.

Acknowledgements

I would like to express my sincerest gratitude to my supervisor Dr. Allan D. Spence for his extensive guidance, support, and encouragement during this research project. As an honourable and knowledgeable professor, he has always been the mentor during my undergraduate and graduate studies. It is a pleasure to deliver my appreciation to him.

I would like to thank the members of Mechanical Engineering Department and colleagues in Dr. Spence's research group for their help and sharing their experiences.

Finally, I would like to thank my parents and girlfriend, Chieh, for their love, support and guidance through my studies and throughout life. The admiration and love I have for them is beyond any words.

Table of Contents

List of Tables

List of Figures

Nomenclature

CAD	Computer Aided Design
CCS	CAD Coordinate System
CMM	Coordinate Measuring Machine
HTM	Homogeneous Transformation Matrix
MCS	Machine Coordinate System
OLS	Orthogonal Least Squares Fitting
PCD	Point Cloud Data
PCS	Part Coordinate System

Chapter 1

Introduction

1.1 Motivation for this Work

The traditional design of large scale aeroengine fan blades involves an interlocking mechanism consisting of a dovetail (or fir tree) attachment at the blade root and the corresponding groove at turbine hub and shaft. This approach provides for ease of assembly and future repair, but is susceptible to wear and fatigue damage that is difficult to repair and normally results in a scrapped blade. Moreover, the dovetail design increases the overall aeroengine weight, decreases the engine performance, and increases the operation cost. Therefore, a new manufacturing method for large fan blade assemblies is desired.

Joining blade and shaft by welding is one of the new methods that have been applied in many military and commercial aeroengines. Because the manufacturing process of complex blade components usually involves multiple stages, including heat-treating, welding, forging, etc., misalignment of the joined blade and hub/shaft can occur.

As a result every component is different and requires post-weld machining to recover geometry as close as possible to the nominal CAD model. Figure 1.1 shows the geometric comparison of a blade CAD model and a laser digitized or scanned model of a misaligned blade assembly cross-section. Because of the misalignment, the nominal CAD model is no longer suitable for tool path generation for post-process machining. Moreover, the excess material from the additive welding process obstructs direct tool path generation from the scanned model. Therefore, in order to generate correct tool path for post-weld machining, a new approach based on the nominal CAD model and the scanned data is introduced in this thesis.

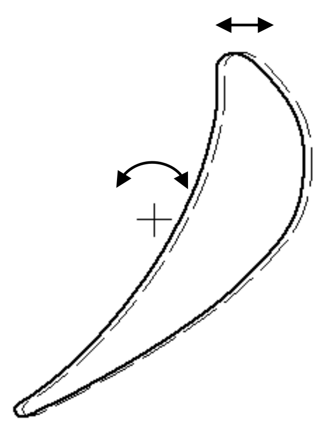

Figure 1.1. Misaligned blade assembly

1.2 Thesis Objectives

The objective of this thesis is to develop a complete workflow to solve the part-to-part variation of joined fan blade and move toward the goal of high speed, high accuracy, low scrap rate refurbishment system. Due to the complexity of blade geometry, the system requires a series of development cycles involving the cooperation and integration of two independent systems - a scanning laser digitizer and CNC machine tools. This requires a specialized CAD/CAM kernel to establish the connection and develop the necessary mathematical algorithm for data processing. The developed workflow can be extended to other applications, such as geometrically deformed moulds and dies after heat-treatment.

1.3 Contributions of this Thesis

The significant contributions described by this thesis include:

1. System design and workflow for a post-process machining process of the joined blade assembly
2. Cross-functional systems integration of laser digitizer and CNC machine tool without significant hardware upgrade
3. Algorithms to robustly generate tool path for solving part-to-part variation issue of the misaligned blade assembly
4. Minimization of the manual grinding process to improve efficiency, accuracy and precision
5. Easy to adapt workflow for other engineering applications, such as mould repairing

1.4 Scope of Thesis

The remainder of the thesis is organized as follows:

Beginning in Chapter 2, typical manufacturing methods for the blade and hub/shaft design are reviewed. A new manufacturing approach by welding is then introduced to reduce repairing cost and improve life cycle. Background information on repairing welded blades is provided, including surface geometry acquisition technologies, data registration methods and tool path generation techniques. The employed CAD/CAM kernel system is presented to handle sophisticated mathematical calculation.

Chapter 3 provides the general architecture of the proposed refurbishment system. The overall data processing methodology is introduced, followed by description of major sub-systems, including the rotary type laser scanner, the data processing PC and CNC machine tool.

Chapter 4 presents the detailed refurbishment workflow based on the proposed system architecture. The workflow includes an algorithm developed to modify the nominal tool path to solve the part-to-part variation of blade-disk assembly. Process details for extracting the nominal tool path and coordinate transformation are also described.

Chapter 5 validates the refurbishment workflow through series of machining experiments. Testing results are digitized and compared with CAD models.

Chapter 6 concludes the thesis and presents suggested future work.

Chapter 2

Literature Review

2.1 Blade Design and Manufacturing

The physical properties of blades are strongly influenced by manufacturing technology and material selection. Blade manufacturing involves a multistage process including, based on the size and application, casting / forging and machining. Stainless steel is the most common material of compressor blades. Material choices include stainless steel and highly alloyed metals including nickel, cobalt, chromium, titanium, molybdenum and tungsten. In this section, blade design and manufacturing technology will be reviewed.

2.1.1 Conventional Dovetail / Fir-Tree Design

The conventional dovetail / fir-tree blade design (Figure 2.1) is susceptible to fretting wear that occurs from vibration induced oscillation forces between two contacting components [1]. Fretting results in wear and high local stress concentration near the edge of contact, and leads to propagation of cracks and reduction of fatigue life [2]. Fatigue failures caused by fretting have become a major concern in aircraft components because of the high maintenance costs. In a turbofan engine application, the dovetail of blade and disk attachment is the most common location of fretting damage due to high rotational force and close fit of joint. Additionally, fretting fatigue in dovetail joints has been recognized as one of the most difficult and costliest source of high cycle fatigue in the US Air Force [3]. Different designs of blade root attachment, such as fir-tree geometry shown in Figure 2.2, have been implemented to minimize the effect of fretting fatigue. Researchers and industry continue to seek an alternative design to replace the conventional blade and hub/shaft mechanical attachment design.

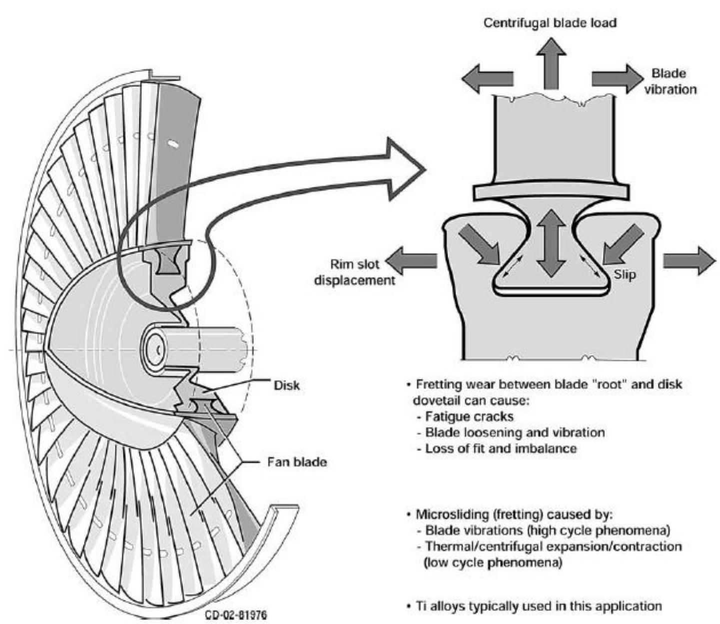

Figure 2.1. Fan and compressor blade dovetail displacements [4]

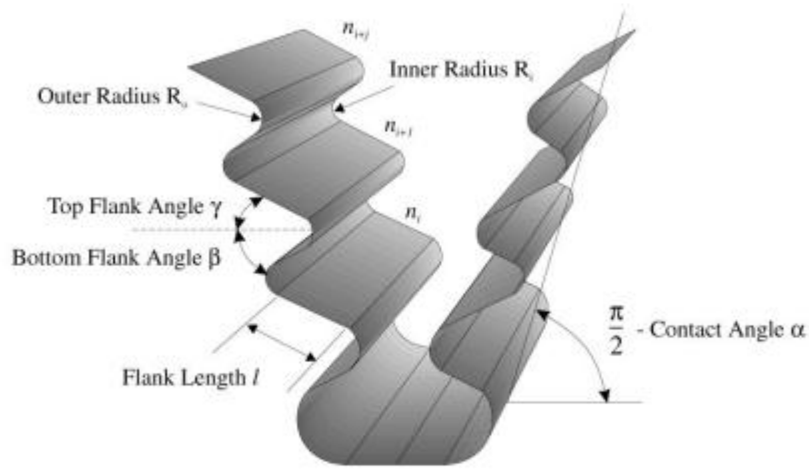

Figure 2.2. Schematic of fir-tree blade root [5]

2.1.2 New Blade Assembly Design and Manufacturing Technology

In order to improve performance and reliability, some recent studies also focus on the new design of the blade assembly structure known as bladed disks (Blisks), or integrated bladed rotors (IBRs) that eliminate the dovetail joint and associated fretting fatigue. The structure of mechanical attached blade-disk and blisk are compared in Figure 2.3 [6]. Starting in mid-1980s, blisks have been employed in the design of military and civil aero-engines, for example: Pratt & Whitney's PW6000 commercial turbofan engine for Airbus A318, Eurojet's EJ200 military turbofan engine for Eurofighter Typhoon and Europrop International's TP400 turboprop engine for Airbus A400M [7].

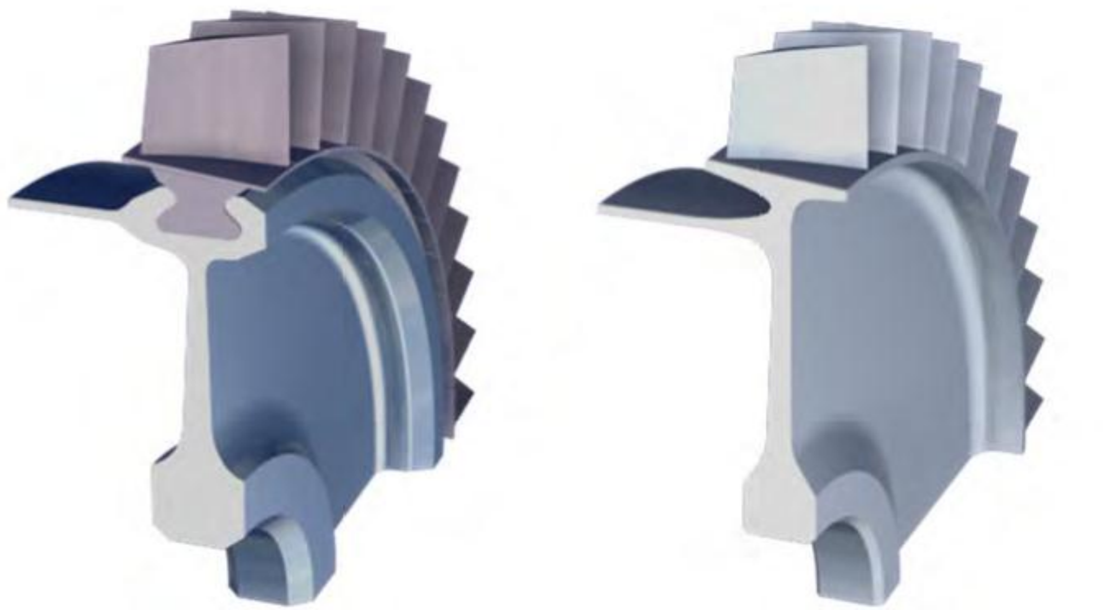

Figure 2.3. Structure comparison of mechanical attachment blade-disk and blisk [6]

Compared to the conventional assembled blade and disk counterparts, the design of blisks has significant advantages as following: [7] [8]

- weight reduction by 20 to 30%
- improvement of aerodynamic efficiency
- reduction of fuel consumption and emission

The reduction of structure complexity and component weight of blisks substantially improves the reliability and performance of aero-engines, and results in reduced hardware life cycle cost. [9] The study done by MTU Aero Engines GmbH has forecasted the growth of blisks market in commercial aero-engines (referring to Figure 2.4) because of the reliable structure and improved thrust-to-weight ratio. However, high manufacturing costs and machining/repairing difficulty are the major challenges for industry. Single piece design remains impractical for larger diameter fan blades. Based on the overall engine / fan blade diameter, manufacturing of involves the following manufacturing process [8]:

- joining process
- machining process
- electrochemical machining (ECM) process

This thesis concentrates on only the joining and particularly machining processes.

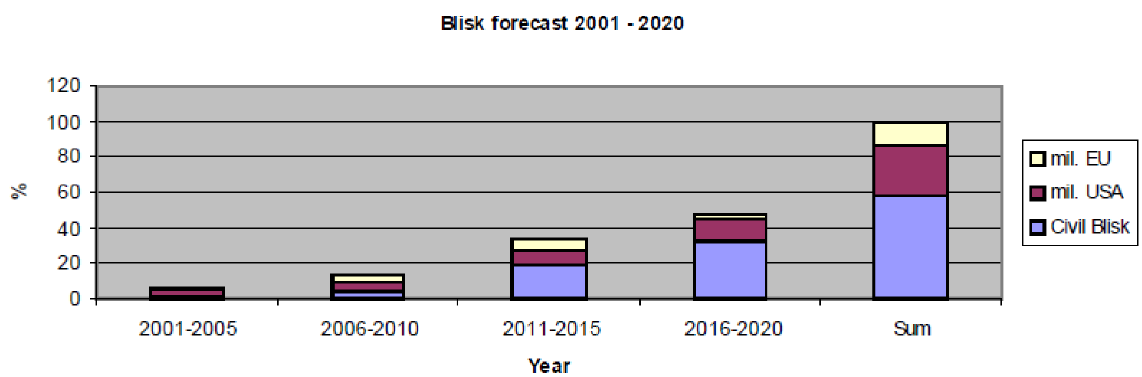

Figure 2.4. Blisk demand forecast 2001 - 2020 [8]

2.1.2.1 Joining Process

The joining process assembles separately machined/forged blades and disks together by welding. This is then followed by adaptive NC machining to remove excess weld material. The approach is most suitable for large diameter fan blades. The fan blade for the Joint Strike Fighter (JSF) System Development and Demonstration (SDD) phase by Rolls-Royce is an example of an assembly manufactured by joining. Compared to machining only, the welding process is capable of joining blades and hub disks made from different materials. The joining process can also be employed for refurbishment to increase the life cycle and reduce repair cost.

2.1.2.2 Machining Process

The machining process involves NC machining of blades and disk on five-axis machine tools. Compared to joining processes, the reliability of only machined blisks is higher. Therefore, smaller compressor blisks are usually manufactured exclusively by machining. Because of difficult to machine titanium and nickel materials, the high cutting forces can result in geometrical deformation of thin-walled airfoils. Therefore, a multistep joining and machining process is usually employed in manufacturing of larger diameter blade assemblies.

2.2 Review of Blade Refurbishment Technology

In the previous section, the design and manufacturing technologies of blades have been reviewed and compared. The joining process of blisks is a new method, which serves to lower manufacturing and refurbishing cost of large scale fan blades. Although the refurbishment technology of joined fan blades slightly differs from convention, the conventional method concepts can be adapted and adjusted for joined fan blades repairing. In this section, conventional refurbishment technologies will be reviewed.

2.2.1 Conventional Refurbishment Technology

For a conventional attached blade, the most common repairing approach of blade is welding with the combination of manual machining or grinding. Manual processes may produce a visually pleasing result. However, it may be time-consuming and geometrically inaccurate to fulfill the quality standards of aerospace industry [10]. Therefore, industry has been developing advanced automated systems to overcome these disadvantages.

2.2.2 Advanced Compressor and Turbine Blade Tip Profiling

Research of advanced compressor and turbine blade tip repair has been studied by many research institutions and companies [11]. Most of them employed the methodology of single freeform surface digitization and tool path generation with the aim of computerized inspection and recontouring process. The practical steps of blade tip refurbishment systems can be summarized in Figure 2.5 [12] For CNC machining process, tool path travels in latitudinal direction along the blade profile. Freeform surface machining is achieved with multiple layers of blade profile, which relied on blade surface digitization and modelling of the actual blade to generate the machining tool path. The authors claimed that this method greatly improved the efficiency and accuracy of refurbishment process by greater automation and less setup time. However, when dealing with large amounts of sampling data, the efficiency of this method decreases due to long data capturing, processing and calculating period for generating a precise tool path.

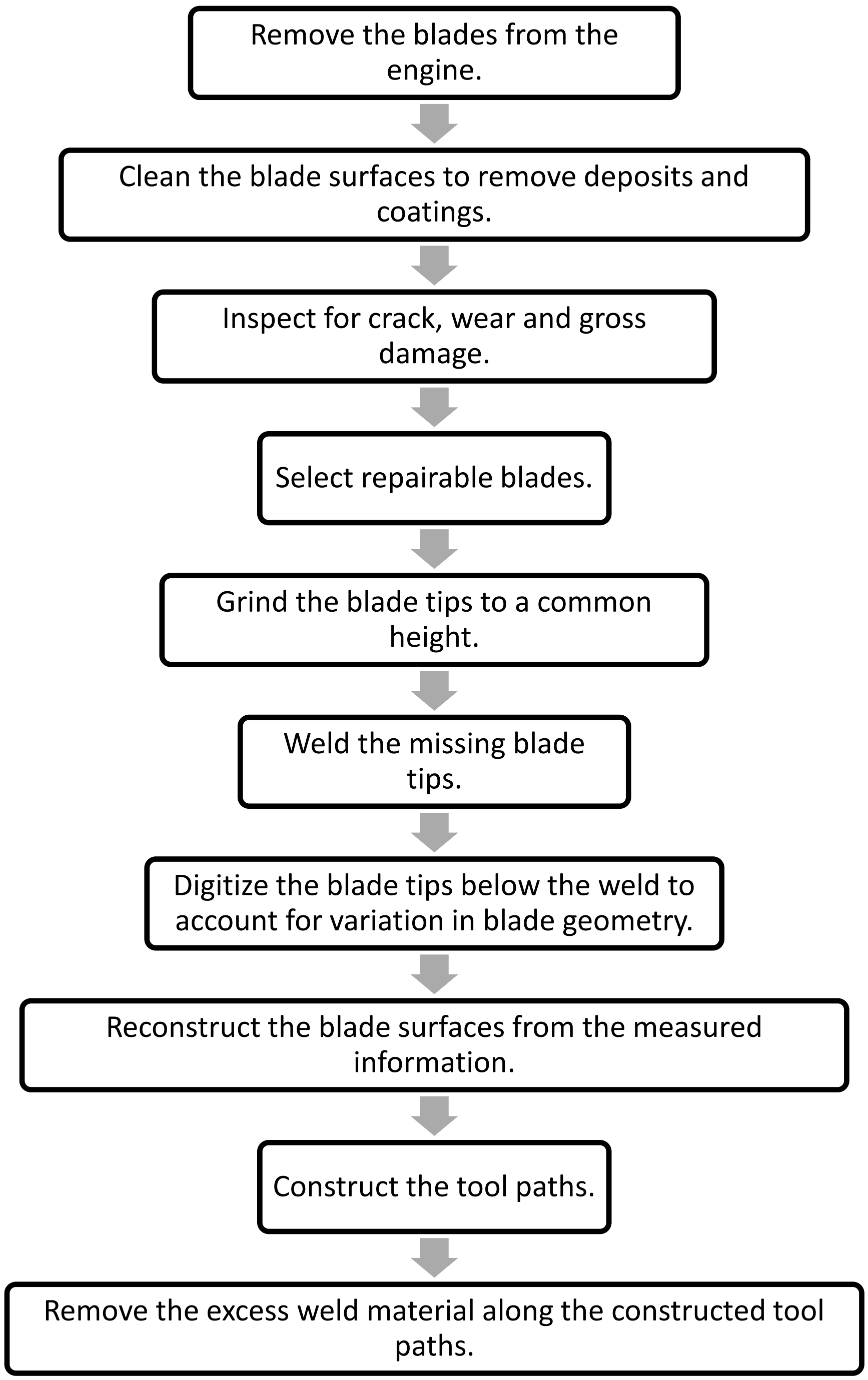

Figure 2.5. Practical steps in refurbishing blade tips [12]

2.2.3 Adaptive Machining Strategy for Conventional Attached Blade Refurbishment

In the last decade, adaptive machining strategy has become very popular for the improvement of conventional blade refurbishment technology. Because blades undergo twist, bow and shift during service, the geometry of every blade is different, and coordinate measurement is required. The nominal CAD model cannot address the change of blade geometry. Therefore, adaptive machining can be employed to adapt the geometric data to accommodate the changing conditions and combine with the nominal CAD model. In order to cope with subtle part-to-part variation, Walton from TTL proposed the adaptive machining strategy by scanning the blade section profile adjacent to the weld bead and modifying the programmed tool path using special software and an attendant computer integrated with three or five-axis CNC machine control [13]. A typical adaptive machining cycle of TTL system is capable of digitizing, computing and restoring the welded blade tip profile in under two minutes, which greatly improves the refurbishment efficiency [14].

Bremer from BCT introduced the similar machining solution. After precise scanning, the scanned data is processed and best-fit with the nominal CAD geometry for generating the adapted NC programs. The BCT adaptive machining system is capable of compensating part-to-part variation and inaccurate clamping positions of complex components.

The refurbishment methodologies and systems mentioned above can only deal with blade outside tip or edge. The tool path is constructed based on the geometric information of a single surface. For joined fan blade manufacturing and repairing, weld material is located closed to disk in order to maintain blade position. Therefore, geometric data of both blade and disk surfaces is needed. This thesis work employs an adaptive machining methodology similar to blade tip refurbishment to solve the part-to-part variation problem of joined fan blades.

2.3 Surface Geometry Acquisition Technologies

The accuracy of the resulting tool path mainly relies on data acquisition. It is very important to acquire accurate and precise surface geometry. Different types of data acquisition systems have been developed to overcome the diverse physical constraints, such as material, size and complex feature. As shown in Figure 2.6, the data acquisition systems can be categorized into two main streams: contact and non-contact technologies. In this section, these fields of technologies will be briefly reviewed and compared.

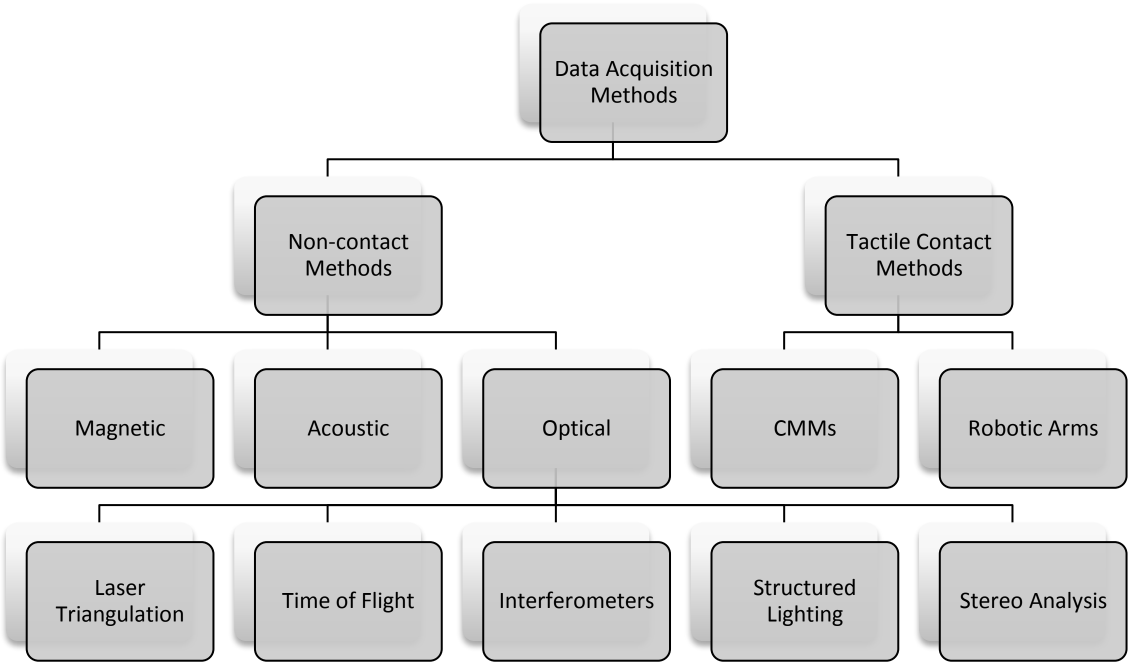

Figure 2.6. Classification of various data acquisition technologies [15]

2.3.1 Contact Technologies

Contact methods usually involve a touch trigger probe to contact the surface of workpiece and record the absolute position of the probe tip's center in the three dimensional Cartesian coordinate system (x, y, z). The measuring device can be mounted on traditional fixed Coordinate Measuring Machine (CMM) or portable articulated arm depending on application requirements. Figure 2.8 demonstrates a typical inspection process of CMM. Compared with the vision based non-contact devices, a CMM has much higher accuracy, and is not limited or affected by viewpoint or lighting conditions [16]. Moreover, the touch trigger probe can easily be retrofitted onto the CNC machine tool. Figure 2.7 [17] represents the schematic of Renishaw M12 probe system, which will be implemented for registration purpose later in this thesis.

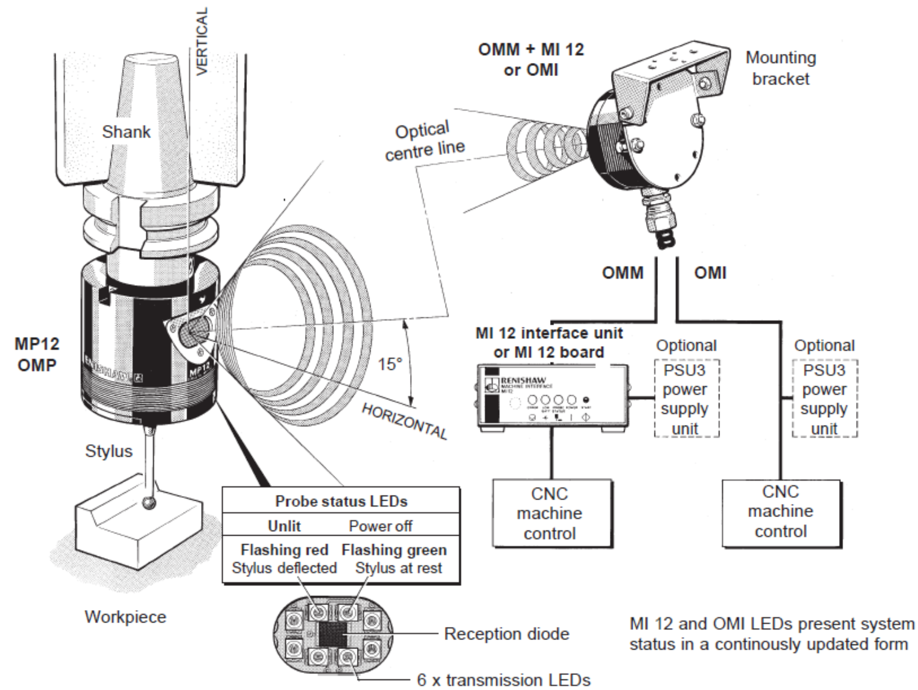

Figure 2.7. Schematic of the Renishaw MP12 probe system [17]

However, several disadvantages limit the data acquisition process using contact technologies. Since this method requires physical contact between probe and measuring object, surface damage to either the probe or part being measured can occur. Inefficient data collection is another disadvantage of contact devices. The touch-trigger technology is a single-point measuring method, which can only achieve a maximum rate of 50 to 60 points per minute. Advanced analog scanning probe technology was developed to dramatically improve the scanning rate by thousands of data points per minute. Comparing to touch-trigger type, analog scanning is a continuous method, that the probe remains in contact with the workpiece surface and produce analog readings while travelling. However, each inspection requires unique setup and NC programming to define the sampling route, which increases the sampling time further [18]. Because of these limitations and constraints contact measuring probe methods are usually chosen only for low density and simple geometries.

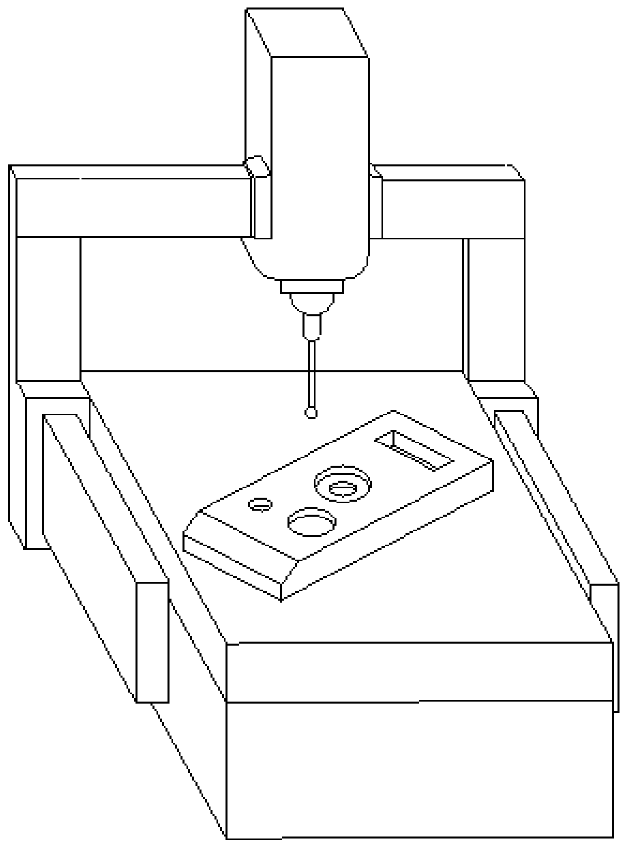

Figure 2.8. CMM inspection

2.3.2 Laser Digitizer (Non-Contact Technologies)

In the case of a workpiece containing multiple complex features, high density and non-contact methods are preferred. In addition, optical type non-contact scanning technology has a very fast measuring speed exceeding 20000 points/s – much greater than contact scanning technology. Recent development of commercial optical type systems has improved the accuracy to about 0.025 mm. [19] [18].

A typical high-density, non-contact digitizer contains a laser that emits light in the form of a spot or stripe onto the measuring workpiece. The reflected light can then be sensed by one or two sensors or charge-couple device (CCD) cameras and stored as intensity data in pixels, which is converted and analyzed to determine the three dimensional coordinates for scanned points on workpiece. The techniques of analyzing position include triangulation, time of flight, and interferometry. The triangulation technique has been widely implemented in high-density, non-contact digitizers. Referring to Figure 2.9 [20], with known projection and collection angles relative to the baseline, the coordinate of a point on the workpiece can be determined by analysing the dimension of a triangle. If a stripe-type laser beam is emitted onto the surface of scanning object, multiple points can be acquired at once, improving the rate of data acquisition.

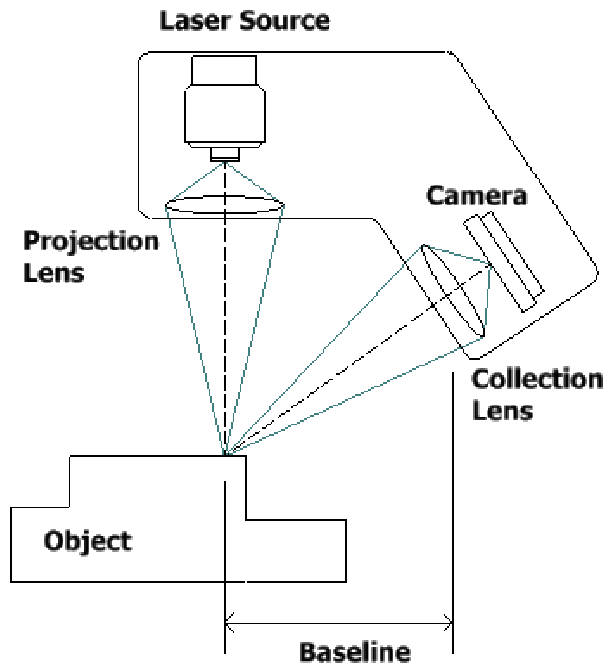

Figure 2.9. The basic principle of triangular-based laser digitizer

The non-contact laser digitizer can be further categorized based on the configuration of the platform. The selection of platform depends on the characteristics of scanning object and the corresponding application. Figure 2.10 [21] presents three of the most popular configurations. The scanning system shown in Figure 2.10(a) shares the same methodology of a typical three-axis milling machine and CMM - the scanning device travels in three perpendicular linear axes. The accuracy of this type of configuration usually outperforms other types due to structural stability of platform.

The second type of scanning system features rotary table and scanning device as presented in Figure 2.10(b). A scanning object mounted on the rotary table, while a stationary or rotating scanning device digitizing its contours. Either the rotary table or scanning device travels along the Z axis in a stepwise manner to incrementally obtain the complete geometric information.

The design of the third type as presented in Figure 2.10(c) integrates the scanning device into an articulated robot arm, which is operated manually by skilled technicians. This configuration has six degrees of freedom, which allows the scanning device to travel and digitize freely within the work envelope of robot arm. Among all configurations, this type is the most flexible method to digitize an oversized workpiece, such as an automobile, but less accurate due to bending and joint / linkage uncertainty.

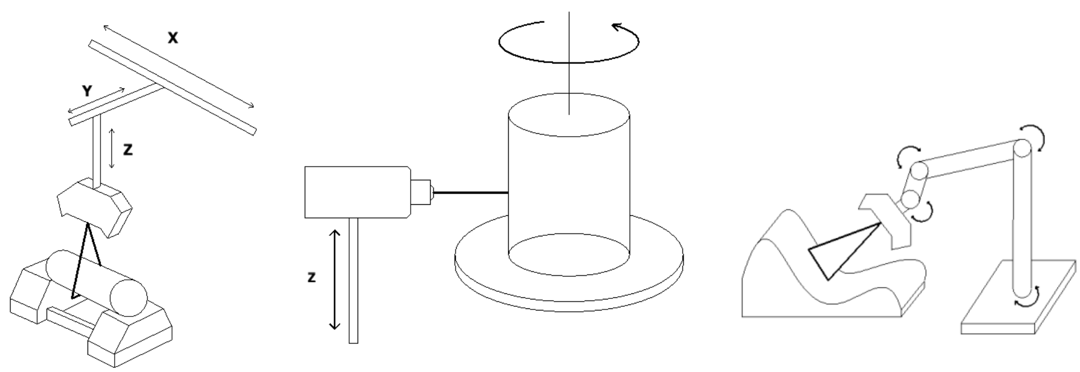

(a) (b) (c)

Figure 2.10. Types of laser scanner configuration

In this thesis work, the laser scanner, Roland LPX-600DS, features triangulation technology and rotary table was first considered and employed for initial process development. This machine is capable of producing dense results with scanning pitch 0.2 mm in width and height direction [22]. As the project proceeding to the next stage with actual size fan blade, a laser scanner integrated CMM or CNC will be implemented due to size and stability requirements.

2.4 Point Cloud and Registration

This section describes the post-processing of acquired measurement data. As described in the previous section, the surface of an object can be modelled by geometrical information collected using a CMM, laser scanner or other digitization device. The collected geometrical information is called point cloud data (PCD). The point cloud data stores the information in 3-dimensional coordinate system. There are two common formats of point cloud data: text files and STL file format, which is the polygonal mesh representation of a point cloud [23].

In the previous section, we introduced some of the most common laser scanning devices and configurations. Although the technology of laser scanning has greatly improved, multiple scanning is essential to ensure flawless data collection. Therefore, registration is required to align and merge multiple scan data. After registration, surface fitting is required for construction of a continuous surface model. The surface model can then be applied for tool path generation. Other applications, such as rendering for product presentation and computer-aided engineering analysis, also depend on surface model [24].

Typical PCD registration is performed for the purpose of 3D model acquisition, object recognition and geometry processing. For optical scanning technology, data acquisition may require multiple scanning from different view angles to capture hidden features. In addition, registration can be employed to perform pairwise alignment of two PCDs by minimization of the squared distance between the underlying surfaces in order to unify the coordinate system between multiple views of a 3D scanned object [25].

Moreover, product quality improvement and scrap rate reduction are critical in modern manufacturing and reverse engineering. The geometry of a machined part or heat-treated mould may deviate from the nominal design model. Therefore, dimensional inspection and tolerance evaluation also require the registration of scanned PCD and nominal CAD model in order to fulfill the functional requirements or assembly conditions [26]. In this thesis, the registration serves to align the coordinate system between PCD and nominal CAD model. This process relies on a homogeneous transformation matrix (HTM) to convert the position vector of point clouds relative to the PCS into the CAD Coordinate System, CCS the coordinate system of the CAD model. Mathematically, the HTM equation is written as [27]:

$$P_{CCS} = [T]P_{PCS} \tag{2.1}$$

where P_{CCS} and P_{PCS} represent the position vector of a point relative to the CCS and PCS, respectively. $[T]$ is a 4×4 HTM:

$$[T] = \begin{bmatrix} t_{11} & t_{12} & t_{13} & t_{14} \\ t_{21} & t_{22} & t_{23} & t_{24} \\ t_{31} & t_{32} & t_{33} & t_{34} \\ 0 & 0 & 0 & 1 \end{bmatrix} = \begin{bmatrix} [R]_P^C & P_{P,org}^C \\ 000 & 1 \end{bmatrix} \tag{2.2}$$

where $[R]_P^C$ is the rotation matrix that represents the orientation of PCS relative to CCS; $P_{P,org}^C$ is the position vector of the origin of PCS relative to CCS. The resulting HTM will be assigned to the coordinate transformation of tool path. To generate HTM, two commonly employed alignment techniques, best-fit and 3-2-1, are introduced below.

2.4.1 Best-Fit Alignment

Best-fit alignment is a common mathematical algorithm employed in many CAD/CAM systems. Conventionally, the registration of scanned data to the CAD model can implies best-fit alignment. The aligned model can be used in many engineering applications, such as dimensional inspection and tolerance evaluation, to improve product quality and reduce scrap rate. The best-fit algorithm employs the Orthogonal Least Squares (OLS) data fitting method to minimize the distance error between pairwise sampling points, which can be simply obtained with tooling spheres. The mathematical functions of OLS can be expressed as following. For a sphere with sample points S_j, center point S and radius r, the orthogonal distance error is

$$d_j = \left[\left(S_{j,x} - S_x \right)^2 + \left(S_{j,y} - S_y \right)^2 + \left(S_{j,z} - S_z \right)^2 \right]^{1/2} - r \qquad (2.3)$$

and the OLS sum to minimize is $\Sigma^2 = \sum_{j=1}^{M} d_j^2$ where M is the number of sphere sample points. Assuming that the sphere is very nearly perfectly round (small form errors), a clever initial approximation is obtained using the linear approximation [28]

$$\begin{aligned}
\theta_j &= \left[\left(s_{j,x} - s_x \right)^2 + \left(s_{j,y} - s_y \right)^2 + \left(s_{j,z} - s_z \right)^2 \right] - r^2 \\
&= \left\{ \left[\left(s_{j,x} - s_x \right)^2 + \left(s_{j,y} - s_y \right)^2 + \left(s_{j,z} - s_z \right)^2 \right]^{1/2} - r \right\} \cdot \left\{ \left[\left(s_{j,x} - s_x \right)^2 + \left(s_{j,y} - s_y \right)^2 + \left(s_{j,z} - s_z \right)^2 \right]^{1/2} + r \right\} \\
&\approx d_j \cdot 2r
\end{aligned} \qquad (2.4)$$

and then minimizing the sum

$$\Theta^2 = \sum_{j=1}^{M} \theta_j^2 = \sum_{j=1}^{M} \left\{ g_j - h - 2 \cdot \left[S_{j,x} S_x + S_{j,y} S_y + S_{j,z} S_z \right] \right\}^2 \tag{2.5}$$

where $g_j = S_{j,x}^2 + S_{j,y}^2 + S_{j,z}^2$ and $h = r^2 - \left(S_x^2 + S_y^2 + S_z^2 \right)$. Simultaneously solving the partial derivative equations

$$\frac{\partial \Theta^2}{\partial S_x} = 0; \quad \frac{\partial \Theta^2}{\partial S_y} = 0; \quad \frac{\partial \Theta^2}{\partial S_z} = 0; \quad \frac{\partial \Theta^2}{\partial h} = 0 \tag{2.6}$$

leads to the linear system

$$\begin{bmatrix} \sum_{j=1}^{M} 1 & \sum_{j=1}^{M} S_{j,x} & \sum_{j=1}^{M} S_{j,y} & \sum_{j=1}^{M} S_{j,z} \\ \sum_{j=1}^{M} S_{j,x} & \sum_{j=1}^{M} S_{j,x}^2 & \sum_{j=1}^{M} S_{j,x} S_{j,y} & \sum_{j=1}^{M} S_{j,x} S_{j,z} \\ \sum_{j=1}^{M} S_{j,y} & \sum_{j=1}^{M} S_{j,x} S_{j,y} & \sum_{j=1}^{M} S_{j,y}^2 & \sum_{j=1}^{M} S_{j,y} S_{j,z} \\ \sum_{j=1}^{M} S_{j,z} & \sum_{j=1}^{M} S_{j,x} S_{j,z} & \sum_{j=1}^{M} S_{j,y} S_{j,z} & \sum_{j=1}^{M} S_{j,z}^2 \end{bmatrix} \cdot \begin{bmatrix} h \\ 2S_x \\ 2S_y \\ 2S_z \end{bmatrix} = \begin{bmatrix} \sum_{j=1}^{M} g_j \\ \sum_{j=1}^{M} S_{j,x} g_j \\ \sum_{j=1}^{M} S_{j,y} g_j \\ \sum_{j=1}^{M} S_{j,z} g_j \end{bmatrix} \tag{2.7}$$

that can be solved for h, S_x, S_y, and S_z. Newton-Raphson or equivalent iterative improvement is then used to minimize $\mathbf{\Sigma}^2$ in the exact problem by solving for δS_x, δS_y, and δS_z in the matrix equation

$$\begin{bmatrix} \frac{\partial \Sigma^2}{\partial S_x} \\ \frac{\partial \Sigma^2}{\partial S_y} \\ \frac{\partial \Sigma^2}{\partial S_z} \end{bmatrix} = \begin{bmatrix} \frac{\partial^2 \Sigma^2}{\partial S_x^2} & \frac{\partial^2 \Sigma^2}{\partial S_x S_y} & \frac{\partial^2 \Sigma^2}{\partial S_x S_z} \\ \frac{\partial^2 \Sigma^2}{\partial S_x S_y} & \frac{\partial^2 \Sigma^2}{\partial S_y^2} & \frac{\partial^2 \Sigma^2}{\partial S_y S_z} \\ \frac{\partial^2 \Sigma^2}{\partial S_x S_z} & \frac{\partial^2 \Sigma^2}{\partial S_y S_z} & \frac{\partial^2 \Sigma^2}{\partial S_z^2} \end{bmatrix} \cdot \begin{bmatrix} \delta S_x \\ \delta S_y \\ \delta S_z \end{bmatrix} \tag{2.8}$$

and then updating the sphere center estimate using $S_x = S_x - \delta S_x$, $S_y = S_y - \delta S_y$, and $S_z = S_z - \delta S_z$. The improved radius estimate is

$$r = \frac{1}{M}\sum_{j=1}^{M}\left[\left(S_{j,x} - S_x\right)^2 + \left(S_{j,y} - S_y\right)^2 + \left(S_{j,z} - S_z\right)^2\right] \tag{2.9}$$

Iterations continue until the estimates for S_x, S_y, S_z, and r converge. Note that convergence is to a relative extreme, and this might be a maximum rather than a minimum. Using the linearized initial approximation, with small form errors, practically eliminates this possibility.

2.4.2 3-2-1 Alignment

An alternative 3-2-1 alignment approach is commonly applied in coordinate registration and is available in most commercial alignment software. The methodology is to constrain the six degrees of freedom of the test object with the reference object (CAD model) using three orthogonal reference datums. Referring to Figure 2.11, the first plane is constructed by measuring or selecting three points from the first datum, i.e. plane Xo-Yo. Similarly, the second plane perpendicular to the first plane is established by measuring two points from the second datum, i.e. plane Xo-Zo. Finally, the third plane perpendicular to the first two planes is established by measuring a point from the third datum, i.e. plane Yo-Zo [19]. The coordinate system of the test object is then aligned with that of reference object by matching the corresponding reference planes. After alignment, the resulting HTM will be applied in the transformation of tool path coordinate system.

For most of the free-form components, datum features are not available on the workpiece, and 3-2-1 alignment technique cannot be directly employed for registration [29]. In this thesis, the design of the simulated blade consists of datum planes for the application of 3-2-1 alignment. For five-axis machining strategy in the future, the engine disk will provide the necessary datum for the alignment purpose.

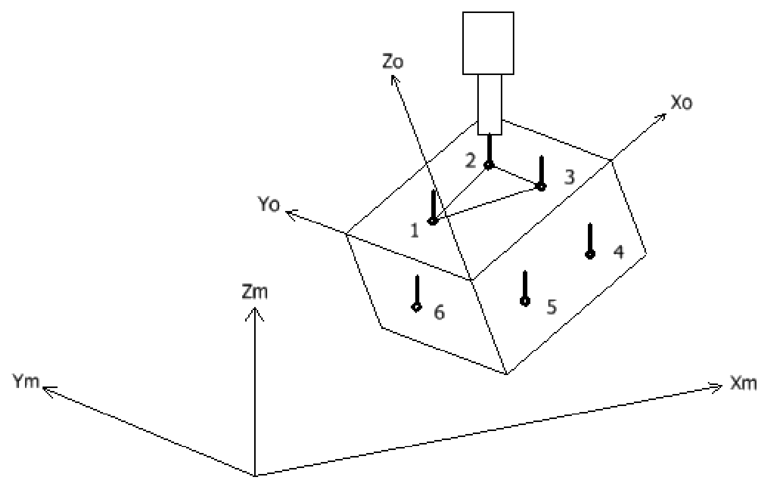

Figure 2.11. 3-2-1 alignment approach

2.5 Tool Path Generation Methods

The early stages of product development flow usually include design concept, prototype, and CAD modelling. The process of product development can be categorized into forward engineering and backward engineering. For forward engineering, the design concept is directly transformed into CAD model in a CAD platform. For backward engineering, the design is first prototyped by design engineers, and then digitized the geometry into CAD data for modelling. Chui et al. [24] compares the general workflows as shown in Figure 2.12. After approval of product design, the manufacturing engineers need to design the most cost efficient manufacturing processes. In general, both forward and backward engineering require machining processes to achieve a specified standard or function. With the aid of commercial CAM software, tool path generation for forward engineering is simple and straightforward. However, the tool path generation for reverse engineering requires surface fitting and modelling of scattered points. Details of different tool path generating method will be discussed in the following sections.

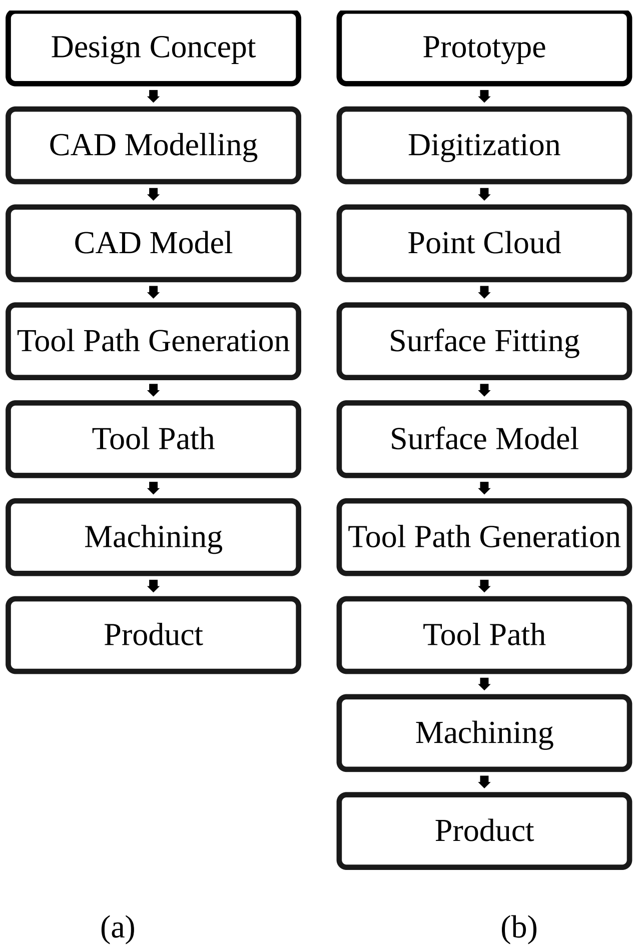

Figure 2.12. (a) forward engineering; (b) backward engineering

2.5.1 Tool Path Generation for Polyhedral Model by Surface Fitting

Conventionally, scattered PCD cannot be implemented directly in the generation of tool path because the lack of parametric information, such as surface normal and curvature. Polyhedral (or triangular facet mesh) models created from measured data points have been widely studied for the generation of tool paths. The techniques of creating polyhedral models usually involve surface fitting of data points. Herein, some of the surface fitting techniques and the corresponding tool path generation methods are reviewed in section 2.5.1.1 and 2.5.1.2 respectively.

2.5.1.1 Surface Fitting Techniques for Generation of Polyhedral Mesh

Lee et al [30] fitted the four corner points from measured data by employing the Ferguson surface model with the following equation:

$$P(u,v) = [F_1(u)\ F_2(u)\ F_3(u)\ F_4(u)] \times \begin{bmatrix} P_{00} & P_{01} & P_{00}^{v} & P_{01}^{v} \\ P_{10} & P_{11} & P_{10}^{v} & P_{11}^{v} \\ P_{00}^{u} & P_{01}^{u} & P_{00}^{uv} & P_{01}^{uv} \\ P_{10}^{u} & P_{11}^{u} & P_{10}^{uv} & P_{11}^{uv} \end{bmatrix} \times [F_1(v)\ F_2(v)\ F_3(v)\ F_4(v)]^T \tag{2.10}$$

where P_{00}, P_{01}, P_{10} and P_{11} are the corner points of surface patch and $P_{00}^{uv} = P_{10}^{uv} = P_{01}^{uv} = P_{11}^{uv} = 0$ [24]. The Ferguson surface patch is then fit as shown in Figure 2.13 and a polyhedral model is created by connecting all surface patches.

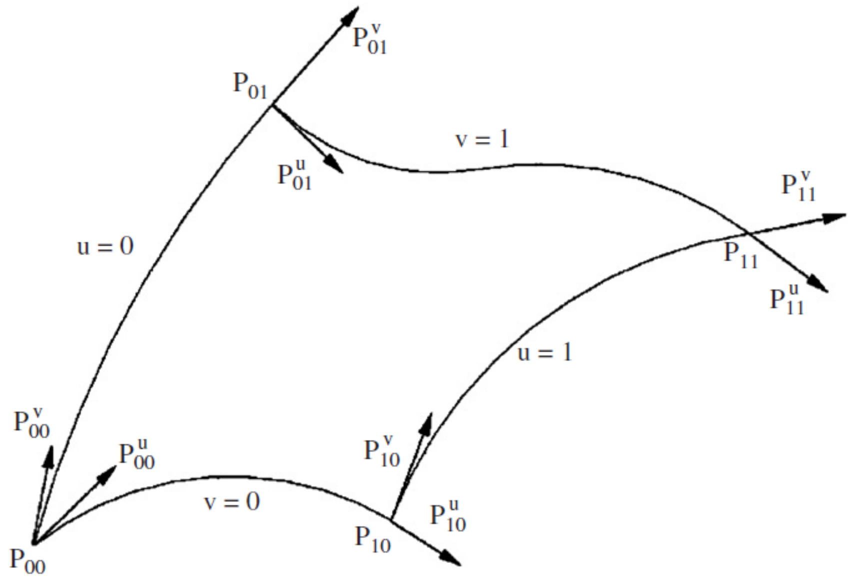

Figure 2.13. Ferguson surface patch [24]

Another approach of surface fitting was studied by Kawabe et al. [31], who employed an offsetting algorithm and a cubic Bezier surface to fit the point clouds using the equation [24]:

$$P(u,v) = \sum_{i=0}^{3}\sum_{j=0}^{3} B_{i,3}(u) B_{j,3}(v) P_{i,j} \quad u,v \in [0,1] \tag{2.11}$$

where $B_{i,3}(u) = \frac{3!}{i!(3-i)!} u^i (1-u)^{3-i}$ and $B_{j,3}(u) = \frac{3!}{j!(3-j)!} v^j (1-v)^{3-j}$

As seen in Figure 2.14, the methodology was to fit and intersect two sets of orthogonal Bezier curves by passing through measured data points along the traces 1 to 4 and a to f respectively. The Bezier curves are the boundaries of each segmental surface patch.

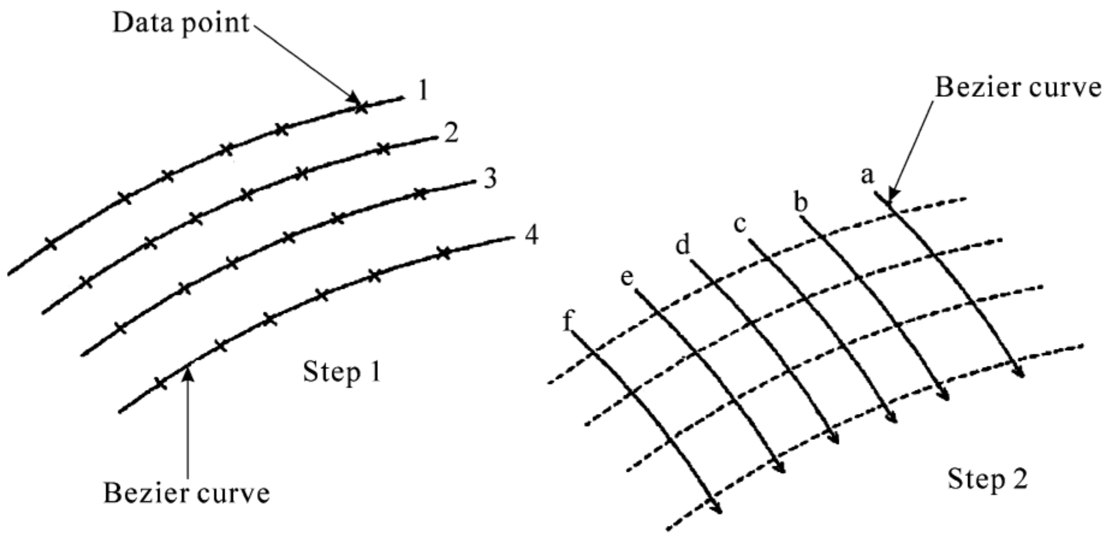

Figure 2.14. Bezier surface patch [24]

Besides surface fitting techniques, in the past decade researchers have focused on triangulation by connecting three non-collinear points. Different algorithms and rules of triangulation have been developed to prevent invalid facet generation. [32] [33]. Details of each algorithm are outside the current thesis scope.

2.5.1.2 Tool Path Generation

Traditional tool path generation methods include iso-parametric and iso-planar. The iso-parametric was first introduced by Loney and Ozsoy [34]. The concept of iso-parametric is to generate cutter contact points along one of the parameters (u or v) of a parametric surface $S(u,v)$, by keeping the other parameter constant. Because the fitted surface can be directly employed in the generation of tool paths, the iso-parametric method has become very popular in freeform surface machining [35]. Another method, which has been widely implemented in commercial CAM software, is iso-planar tool path generation. The methodology of iso-planar is to intersect a triangular facet mesh surface with parallel planes in Cartesian space [36]. However, both iso-parametric and iso-planar methods are considered as non-optimized path planning because of the conservative path interval in term of scallop height k control. Decreasing the step-over interval will minimize the scallop height and lead to better surface finish, but result in longer machining time. Therefore, Suresh et al. [37] and Lin et al. [38] employed the iso-scallop tool path planning method to generate consistent scallop heights over the freeform surface.

2.5.2 Tool Path Generation from Point Clouds

Considering the complexity of surface fitting and triangulation process, methods of direct tool path generation from point clouds have been employed by many researchers. Lin et al. [39] employed the z map approach. The methodology is to reorganize the measured scatter points into rectangular girds in XY plane by interpolation. The mesh point height of any rectangular grid region can then be extracted and linked by line segment for the generation of tool path. Since surface fitting is not required, this method has the advantages in terms of a simpler data structure and faster data processing. However, this method is limited to point clouds in a regular grid.

For the case of irregular grid, Chui et al. [40] proposed the bandwidth method for direct three-axis machining. Their algorithm is to partition scattered points into bands. Each band represents the cutter step-over path. The bandwidth of planar surface is calculated with the following equation:

$$\Delta y = 2r = 2\sqrt{R^2 - (R-k)^2} \tag{2.12}$$

For point clouds from sculptured surfaces,

$$\Delta y = 2r = 2\sqrt{R^2 - (R - k \pm \Delta k)^2} \tag{2.13}$$

where R is the radius of cutter and k is the scallop height. Figure 2.15 shows the approximation of bandwidth. Within each band, spherical surfaces can be created by consecutive pairs of adjacent points for locating cutter positions and tool path generation. This direct machining method omits the time consuming surface generation and triangulation process.

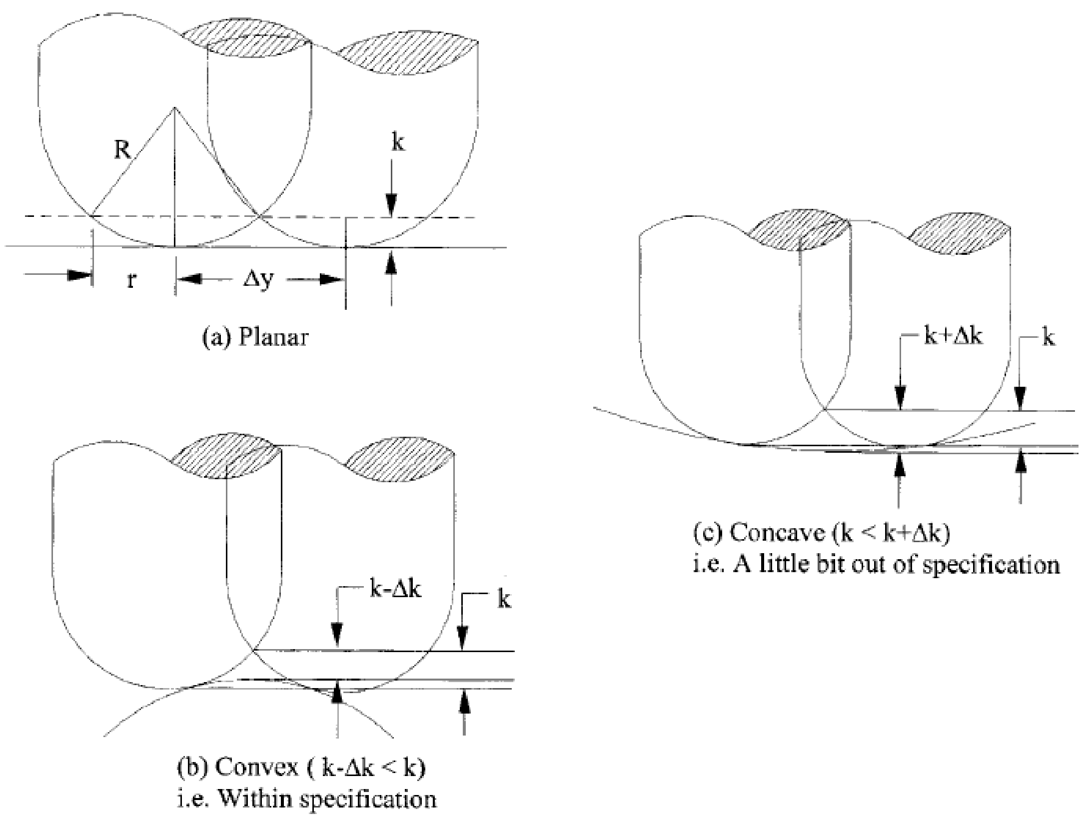

Figure 2.15. Bandwidth approximation [40]

2.6 CAD/CAM Development Software

Since their inception in the 1960s, CAD systems have greatly improved and become very powerful. The framework of a CAD system is briefly described below.

Similar to most computer operating systems, for the design of CAD systems the kernel is the main component. The modelling kernels are usually developed or owned by a single company and can be licensed to other developers for integration of their own CAD programs. Most commercial CAD software were developed based on the modelling kernel, that additional application, features and interfaces were added. In this thesis, the ACIS 3D modelling kernel, developed by Spatial Corporation [41], is introduced for the development of customizing tool path generation. The structure of ACIS kernel is an open, object-oriented C++ architecture, that features robust, 3D modelling functionality and flexibility for achieving application or research requirements. The developed applications are rendered using a 3D graphics toolkit, the HOOPS 3D Graphics System (HOOPS/3dGS) from Tech Soft 3D [42].

2.7 Summary

In this chapter, all applied technologies have been reviewed with the importance emphasized for the proposed fan blade refurbishment process. An overview of blade refurbishment, geometric data acquisition, data registration and tool path generation was presented, followed by the related CAD/CAM kernel required to achieve the thesis objectives. The remainder of this thesis will illustrate the detailed workflow.

Chapter 3

System Architecture

This chapter illustrates the refurbishment system architecture with detailed specifications of major components. The system is constructed by three major sub-systems (see Figure 3.1):

- Laser digitizing system for acquiring surface geometry
- Personal computer (PC) for processing measured PCD, data fitting and customizing tool path
- CNC machine tool for registration and executing the machining tool path

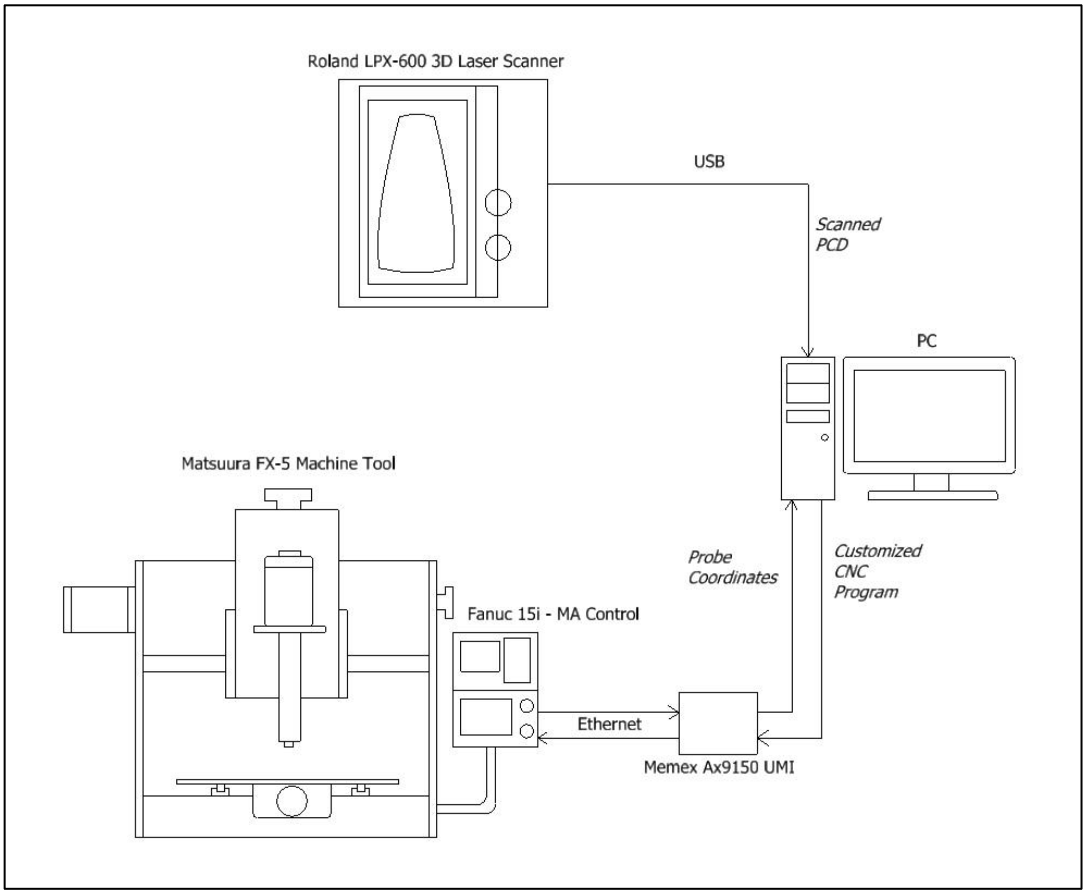

Figure 3.1. Architecture of proposed refurbishment system

The Roland LPX-600 laser digitizing system captures the surface geometry of scanned object [22]. Geometric information will then be passed to the PC over a USB cable. Data is then processed to perform registration and tool path generation through a custom developed ACIS/HOOPS program. The tool path customization methods are described in more detail in Section 4.4.

The CNC machine tool serves two important purposes workpiece registration and tool path execution, which requires uploading registration data and downloading NC tool path from the perspective of machine tool controller. As described in Section 2.3.1, a

Renishaw M12 probe system featuring a touch-trigger probe was integrated with the Matsuura FX-5 Machine Tool to measure datum for coordinate registration. The probing result is exported via the Ax9150 Universal Machine Interface developed by Memex Automation Inc. [43] through Ethernet connection to PC (see Figure 3.1). The Ax9150 UMI is connected to Serial port 1 of the Fanuc Series 15i-MA controller, and then linked to PC via Ethernet and local area network router. The sophisticated probing routines for blade-disk assembly can be created by configuration of the probing cycle programs provided by the probe manufacturer. The measured data will then be processed by commercial inspection software installed on the PC to create HTM, which transforms the coordinate system of the customized tool path. Finally, the resulting tool path is fed back to controller for execution.

Chapter 4

Machining Workflow

Previously, blade tip refurbishment systems were reviewed. Critical steps of these systems include: welding the blade, digitizing the surface adjacent to the weld, constructing the fillet in the weld zone and generating a tool path to machine away excess weld material. In this chapter, a similar machining workflow is introduced for the manufacturing or refurbishing of large scale turbofan blades using a joining process that attaches the blade onto hub / disk by welding. As mentioned before, the challenge in this method is the transition surface smoothness. The emphasis of the proposed workflow is on smooth tool path construction.

The proposed machining workflow is as follows:

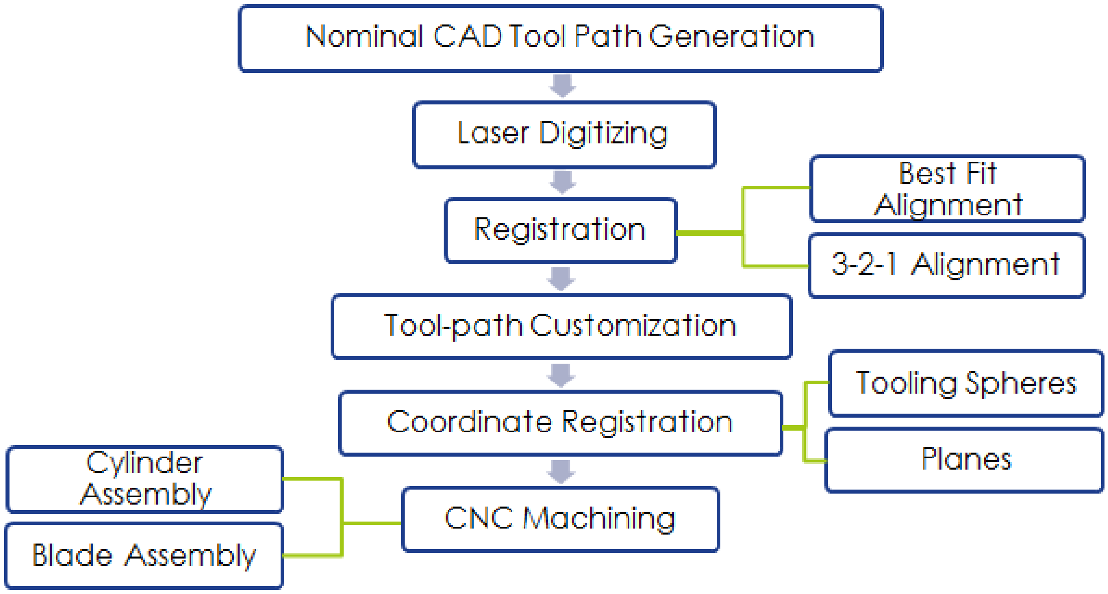

Figure 4.1. Machining workflow

The proposed machining workflow will be validated by three sets of CNC machining experiments, that contain different orientations and blade-disk assembly geometries. The cylinder assembly experiment is for the purpose of concept development. The nominal blade-disk assembly and offset blade-disk assembly experiment is for the verification of machining process. Details of distinct methods will be discussed in Sections 4.3 to 4.5.

4.1 Nominal CAD Tool Path Generation

After assembly and welding, it is common that the blade-disk assembly orientation slightly deviates from the original CAD model. Hence it is necessary to customize the tool path for the part-to-part variation of each blade-disk assembly. In addition, the ultimate goal is to implement the machining strategy on factory floor, where software reliability and simplicity are key factors. Therefore, the customized tool path will adapt the machining strategy and tool path of the nominal CAD model, which has been previously created and saved.

To create the nominal CAD model tool paths, discrete cutter contact points on the final workpiece are calculated. These cutter contact points are determined by applying the conventional iso-parametric method. The nominal CAD tool path cutter center points are found by projecting the cutter contact points by the known tool radius along the outward surface normal. By connecting all cutter center points, the nominal CAD tool path can be created as represented in Figure 4.2. The completed tool path of the blade is shown in Figure 4.3, which covers the zone within the fillet. However, the welding process is performed manually, which results in inconsistent welding area. Therefore, the nominal tool path is further extended into adjacent surfaces as presented in Figure 4.4. The scripts written to generate the nominal tool paths are included in Appendix B.1.

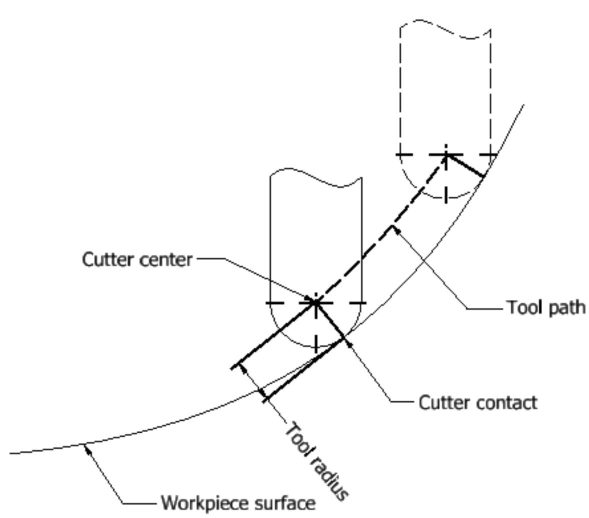

Figure 4.2. Schematic of tool path generation based on surface geometry and tool radius

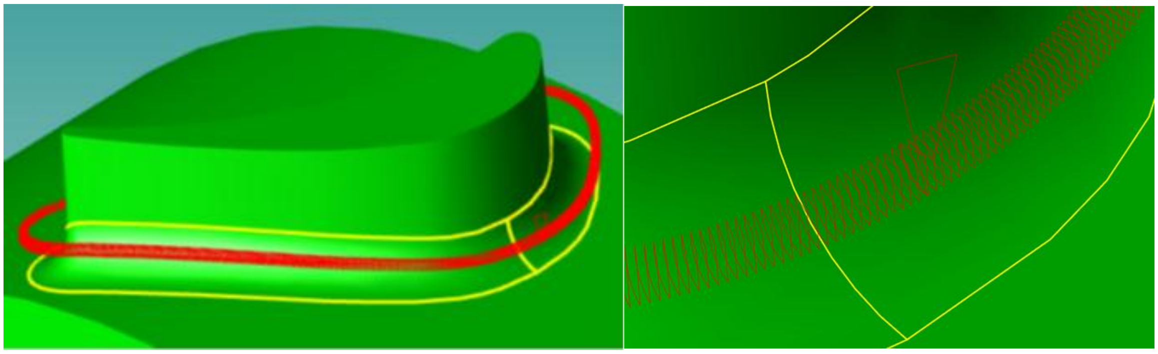

(a) (b)

Figure 4.3. Nominal tool path generation (red line) at transition area using CAD model: (a) global view; (b) zoom-in view

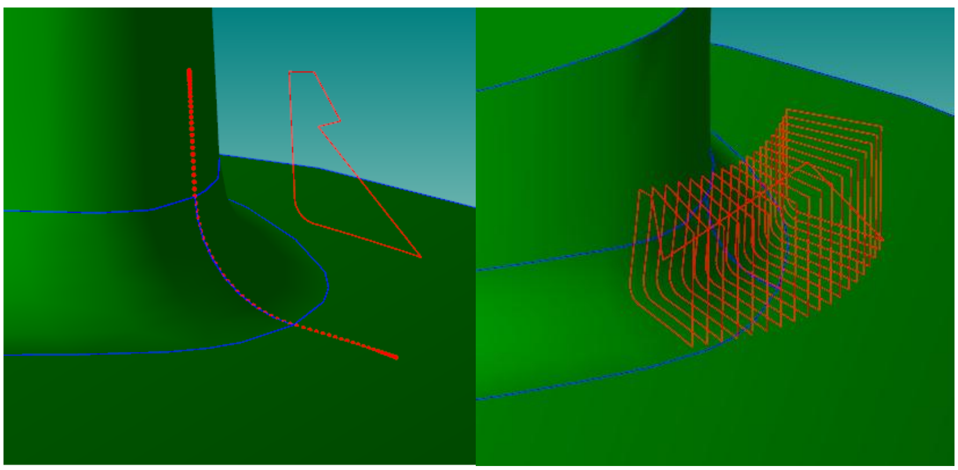

(a) (b)

Figure 4.4. Extended nominal tool path generation (red line) at transition transition using CAD model: (a) single loop; (b) multiple loops

4.2 Surface Laser Digitization

The blade/shaft assembly is then laser digitized into point clouds using a laser scanner system. The applied laser scanning methodology is the spot-beam triangulation as described in Section 2.3.2. The scanning resolution is 0.2 mm in width and height to accurately capture fine distinction of irregular weld surface. Each scanning cycle is approximate 60 minutes. Time varies with the dimension of the scanning field. For presentation purpose, the geometry of blade assembly is entirely digitized, which results in longer scanning cycle. The scanning field in Z axis can be further reduced to acquire necessary geometry only to shorten the scanning cycle. The part to be scanned is sprayed with Magnaflux SKD-S2 developer [44] to minimize the noise of data acquisition during laser scanning.

The digitized data is stored in the form of Point Cloud Data (PCD). Figure 4.5 shows the laser digitized point cloud data of a blade assembly, and consists approximately 120,000 points. Saved point cloud data will be used in the registration of coordinate system and construction of triangular faceted mesh for the assembly. The faceted mesh of assembly will be the foundation of generating customized tool path.

Figure 4.5. Point clouds of blade assembly

4.2.1 Sources of Errors

The digitizing error of the laser scanning process is the combination of random error and systematic error. For a triangulation-based scanner, one of the main sources of random errors is caused by speckle noise in CCD laser images due to the cancellation and reinforcement of the light wave amplitude on the CCD [45]. This effect is caused by wave cancellation or reinforcement and results in dark or bright speckles, respectively. Speckle noise can increase the uncertainties in gathering data and calculating coordinate position, which may result in outliners. Outliers are defined as isolated points deviating from their coplanar neighbouring points by a certain distance. Before any registration and triangulation, acquired data requires manual and/or automated removal of outliers to ensure accurate and repeatable results. Noise reduction features are available in most commercial inspection software. In this thesis work, scanning noise of point cloud data was filtered by using Geomagic Qualify [52], a commercial inspection and metrology software. After construction of triangular facet mesh, noise of polygons could perform additional filtering to remove erroneous spikes to assure accuracy of the triangular mesh.

Systematic error is a repeatable error under the same scanning conditions, which may be caused by the rotary table, the scanner, the fixture, the spray material the part setup method, etc. [46]. Feng et al. [47] claimed that when the systematic error can be accurately predicted by a mathematical model. The accuracy of scanning results can be improved if the associated random error is relatively small.

4.3 Registration

The registration procedure serves a very important purpose, alignment of point clouds and nominal CAD model, by HTM. The theoretical expression of a standard 4 x 4 HTM is described in Section 2.4.

Because of the innovation of laser scanning technology, dense and accurate point clouds can be captured. A very common registration method is to align the point clouds with a set of simple CAD primitives, such as spheres and planes. [48] The registration process herein will be performed by fitting CAD primitives with the corresponding point clouds using commercial inspection software. In order to perform accurate registration, identical reference planes/points must be established in both PCD and CCS. Point clouds and CAD model can then be registered by different aligning methods. In this thesis, two alignment methods, Best Fit and 3-2-1 alignment, will be applied. Procedures are described in the following section.

4.3.1 Best Fit Alignment

For the cylinder assembly experiment, the point clouds are registered with the nominal CAD model by the alignment of tooling spheres. Since this experiment is for verifying and developing of the concept, the cylinder and shaft are assembled according to the nominal CAD model. Offset between the actual assembly and nominal CAD model is minimized and neglected.

As described in thesis objective, the purpose of this refurbishment procedure is to remove excess weld material at blade fillet. After assembly and digitization, the joining region located at blade fillet is covered by weld material. Therefore, the surface registration method must neglect the fillet surface on the CAD model as seen in Figure 4.6. The registration is performed by best-fitting the pairwise center points of tooling spheres between PCD and CAD model. The results of before and after point clouds registration to nominal CAD model are shown in Figure 4.6. The registration method is performed to align the pairwise center points of tooling spheres between PCD and CAD model by Best Fit Alignment, which applied the Orthogonal Least Squares Fitting method. The result is presented graphically as seen in Figure 4.7, which demonstrates excellent alignment between test (PCD) and reference (CAD) objects.

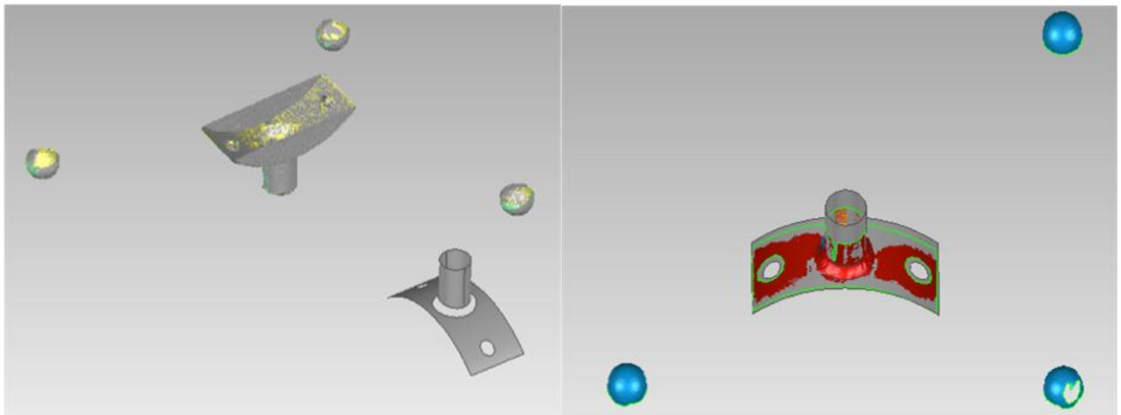

(a) (b)

Figure 4.6. Registration by best fit alignment: (a) before registration; (b) after registration

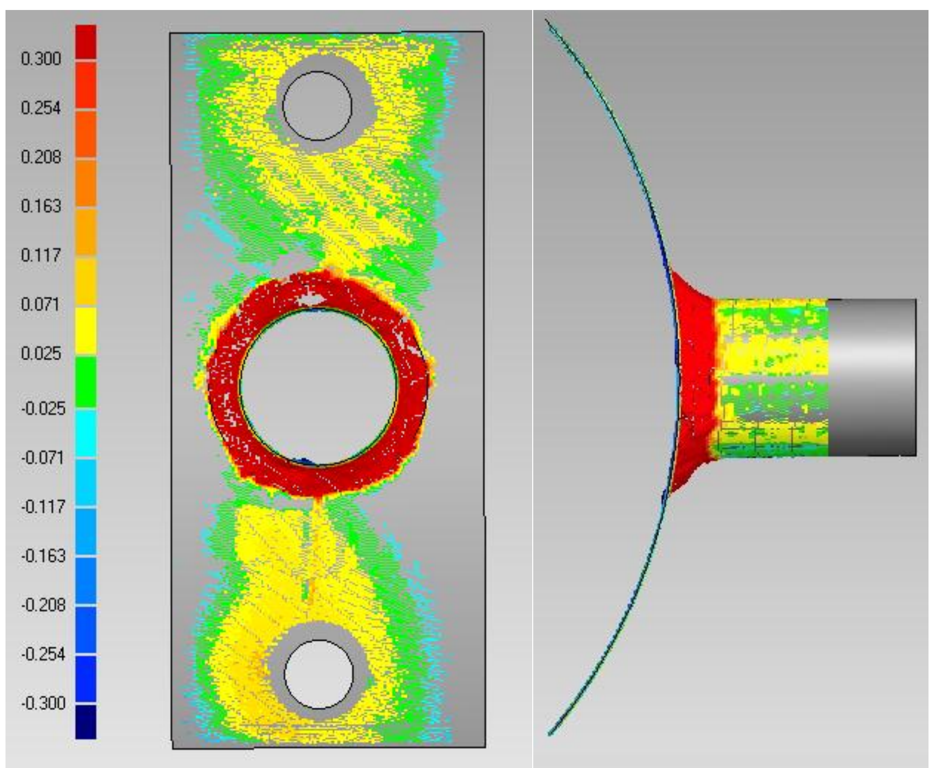

(a) (b)

Figure 4.7. 3D compare of registered PCD and nominal CAD model: (a) top view; (b) side view

4.3.2 3-2-1 Alignment

The methodology of 3-2-1 alignment is to constrain the six degrees of freedom of the part needed to be registered as described in Section 2.4.2. First, a base plane must be created by selecting three points on the datum plane XY. This step will constrain three degrees of freedom: 1) movement in Z axis, 2) rotation about X axis, and 3) rotation about Y axis. Next, create an edge by selecting two points on the XZ or YZ plane to perform axis alignment, which constrains two degrees of freedom: 1) rotation about Z axis, 2) movement in Y or X axis depending on the orientation of edge created. Finally, create a point on the remaining plane to fully constrain the part. The graphic representation of alignment result is shown as Figure 4.8. The blade-disk assembly adapts 3-2-1 alignment to transform its position vector from PCD to CCS.

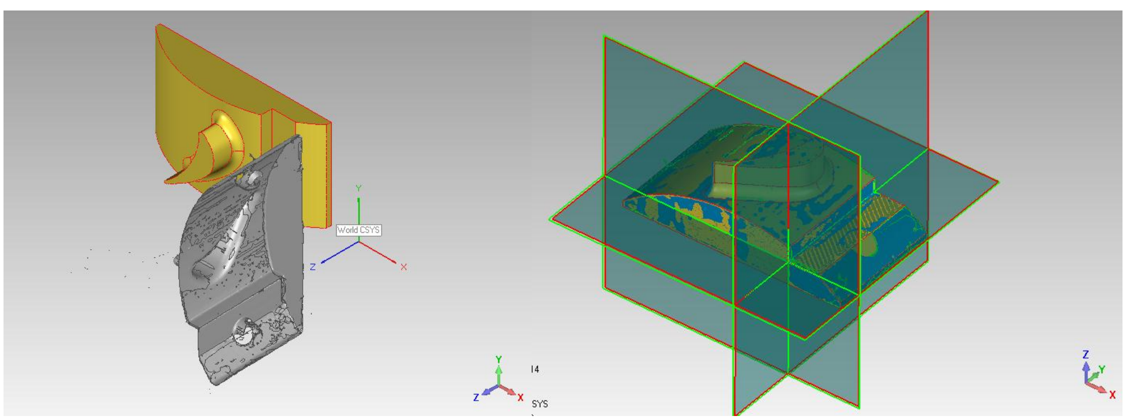

(a) (b)

Figure 4.8. Registration of 3-2-1 alignment: (a) before alignment; (b) after alignment

4.3.3 Summary

Two registration methods, Best Fit and 3-2-1 alignment, were introduced in this section. Best Fit alignment was first considered and implemented on the cylinder assembly test at the process developing stage. This method required laser digitization of additional tooling spheres, which increase the source of error and scanning period due to increased points collection and multiple scanning. Approximately 57,800 points were collected for a 1.5” diameter tooling sphere with 0.2 mm scanning resolution. As the research progressed, 3-2-1 alignment was implemented to replace Best Fit method by adding reference planes at the simulated blade assembly model. (See Appendix A.1 for reference planes on blade assembly.) Registration would rely on reference planes instead of tooling spheres, and better simulates the datums that would be available on a full 360 degree hub assembly.

4.4 Tool Path Customization

The registered point clouds will be used to construct the customized tool path in this section. The purpose of customizing the tool path is to re-construct the continuous surface smoothness of blade/fillet and disk/fillet joints, that is covered by welding material. The re-constructed surface is described by a set of curves, where each curve represents a series of connected cutter contact points within a normal plane. As mentioned in Section 4.1, the cutter contact points represent the contact location of cutter and workpiece in metal cutting process. The cutter contact points are constructed using two different methods: non-uniform rational B-spline (NURBS) and interpolation. Each method requires two sets of intersection points on the facet of blade and shaft surface.

In Section 4.2, triangular facetted mesh of the blade-disk assembly has been created by digitized PCD. Each set of intersection points are found by projecting the nominal vectors through the facets of blade and shaft. Nominal vectors are created by connecting the cutter center and the corresponding cutter contact points found in Section 4.1. Details of tool path customization for each method are described in the following sub-sections. Since the proposed machining method emphasizes removal of extra weld material, the uncut volumes left at the assembly is comparatively small. Therefore, clean-up machining with a smaller cutter radius will be considered in the generation of customized tool path. Despite customization methods, all tool paths are recorded by cutter center points in the three dimensional Cartesian coordinate system (x, y, z) and presented as the following matrix form:

$P = \begin{bmatrix} X_i & Y_i & Z_i \end{bmatrix}$, where *i* indexes through the set of cutter center points.

The scripts written to generate customized tool paths are included in Appendix B.2.

4.4.1 NURBS

As described in 4.4, two sets of facet intersection points on blade (point A – E) and shaft surface (points F – J) are required. For constructing NURBS, each set of five intersection points is used to create a single span least squares fit cubic B-spline represented by S1 and S2 in Figure 4.9. Mathematically, for S1, this is accomplished by denoting the intersection point coordinates $Q_1(x_{Q,1}, y_{Q,1}, z_{Q,1}) = A, \dots, Q_5 = E$. With uniform knot parameters $u_k = 0,1,2,3$ the best fit cubic B-spline has four control points $P_j = (x_{P,j}, y_{P,j}, z_{P,j})$ and the distance from each sample point to the curve is defined as $d_k = \left\| \sum_{j=1}^{4} N_{j,3}(u_k) P_j - Q_k \right\|$ where $N_{j,3}(u_k)$ are the values of the cubic B-spline basis functions at u_k. The least squares quantity to minimize is $\widehat{D} = 0.5 \sum_{k=1}^{5} d_k^2$ and the minimum occurs when the partial derivatives $\partial \widehat{D} / \partial P_j$ equal zero. Expanding

$$0 = \partial \widehat{D} / \partial P_j = \sum_{k=1}^{4} d_k (\partial d_k / \partial P_j) = A^T A P - A^T Q \tag{4.1}$$

where $A = [a_{j,k} = N_{j,3}(u_k)]$, $P = [P_1\ P_2\ P_3\ P_4]^T$, and $Q = [Q_1\ Q_2\ Q_3\ Q_4\ Q_5]^T$.

The solution is found using matrix inversion based on Singular Value Decomposition (SVD) with $A = U \Sigma V^T$. Rewriting (4.1)

$$P = (A^T A)^{-1} A^T Q = V M U^T Q \tag{4.2}$$

where $\Sigma = [\sigma_{i,j}]$ and $M = [1/\sigma_{i,j}]$.

An additional cubic NURBS curve

$$C(t) = \frac{\sum_{j=1}^{4} N_{j,3}(t) w_j P_j}{\sum_{j=1}^{4} N_{j,3}(t) w_j} \tag{4.3}$$

is then created as a continuous curve that is tangent to S1 and S2. To obtain a small G2 fillet radius, the NURBS control point weights used were $w_{j=1\dots4} = 1,10,10,1$.

Then ACIS function *api_mk_ed_int_ctrlpts()* was be used to create the cubic NURBS curve, which is sampled to extract the cutter contact point at fillet area. The cutter center points are then located based on the curve normal and known tool radius. Finally, the customized tool path is generated by joining all cutter center points.

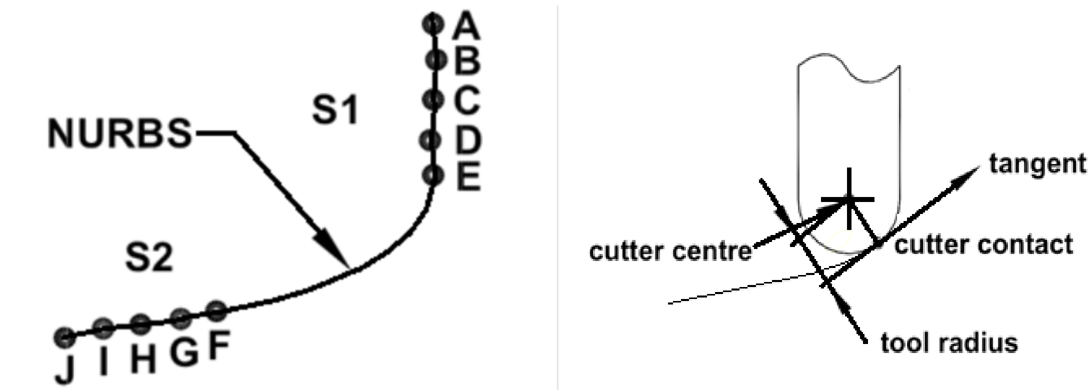

(a) (b)

Figure 4.9. NURBS construction: (a) NURBS curve; (b) cutter centre and contact point

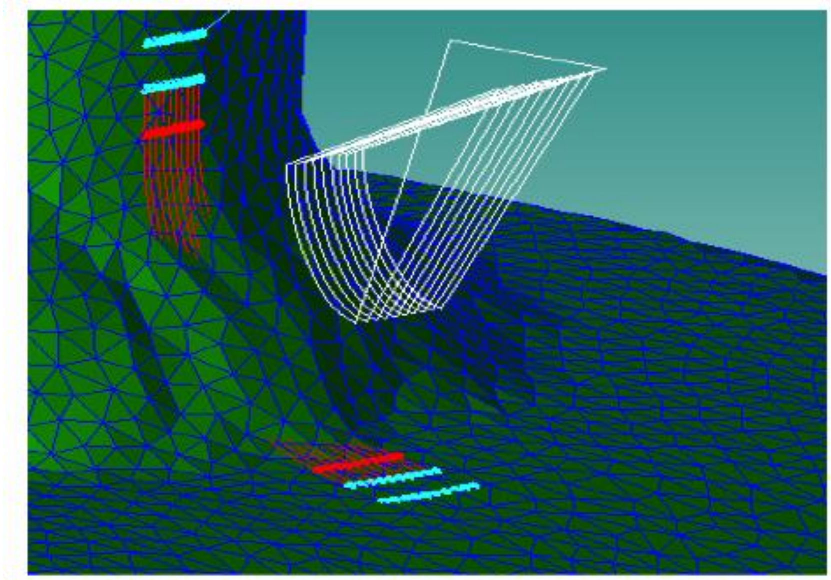

Figure 4.10. Customized tool path by NURBS

4.4.2 Interpolation

Compared to NURBS, interpolation is a simplified method to customize the tool path. It is constructed by using the average offset between the actual blade assembly and the nominal CAD model to interpolate the estimated offset within the fillet region. The customized cutter contact points at fillet will then be calculated based on the nominal cutter contact points and the interpolated offset. The interpolated points along the fillet region are the customized cutter contact points for blade assembly.

The process starts with measuring the offset along blade and shaft of the actual blade assembly. As mentioned in Section 4.2, the actual blade assembly is laser digitized in the form of point clouds, which represent the digitized location of vertices in 3D coordinate system. Point clouds of the actual blade assembly are then converted into a triangular facetted mesh and registered with the nominal CAD model. Similar to the NURBS method, two sets of intersection points on blade and shaft surface will be used in the process. For intersection details refer to the method described in Section 4.4. Each set of intersection points contains ten sampling points, represented by $A_1, \dots, A_{10}$ and $B_1, \dots, B_{10}$ on the blade and shaft surface respectively. Each intersection point has its corresponding cutter contact point on nominal CAD model, $C_1, \dots, C_{10}$ and $D_1, \dots, D_{10}$, on blade and shaft surface respectively. Mathematically, the offset between the intersection and nominal CAD model cutter contact points is defined as $d1_k = A_k - C_k$ and $d2_k = B_k - D_k$ for blade and shaft respectively.

The average offsets of blade and shaft are

$$\overline{d1} = [\sum_{k=1}^{10}(A_k - C_k)]/10 \tag{4.4}$$

$$\overline{d2} = [\sum_{k=1}^{10}(B_k - D_k)]/10 \tag{4.5}$$

The interpolated offset is calculated using (4.4) and (4.5) as

$$d3_j = \overline{d2} + j * \left(\overline{d1} - \overline{d2}\right)/N \tag{4.6}$$

where $j = \{1, 2, \dots, N\}$ and N controls the dense of interpolation.

The customized cutter contact points at fillet region, $E_1(x_{E,1}, y_{E,1}, z_{E,1}), \dots, E_j$, are found by projecting the nominal vector, u, from the nominal cutter contact points, $F_1(x_{F,1}, y_{F,1}, z_{F,1}), \dots, F_{10}$, with the distance of interpolated offset. $\begin{bmatrix} x_{E,j} \\ y_{E,j} \\ z_{E,j} \end{bmatrix} = \begin{bmatrix} x_{F,j} \\ y_{F,j} \\ z_{F,j} \end{bmatrix} + d3_j \hat{u}_j$ where $\hat{u} = u/\|u\|$ and u is the vector connecting the nominal cutter center and the corresponding cutter contact point. The interpolated curve is constructed by connecting all interpolated cutter contact points. The customized cutter center points can be located based on the curve normal and known tool radius. Finally, the customized tool path is constructed by connecting all cutter center points.

4.4.3 Summary

Two customized algorithms, NURBS and interpolation, were implemented in this section for the rough machining process of welded blade assembly. Although both algorithms produced continuously smooth transition, interpolation was preferred in terms of controllability. The theory and methodology of NURBS algorithm is mathematically more complex as comparing to interpolation. Tool path constructed by interpolation can be easily adjusted by manufacturing engineers depending on the industry standard.

4.5 Coordinate Registration

Before executing the customized tool path on the CNC machine, the workpiece needs to be mounted on the CNC machine. The blade-disk assembly is mounted on a specially designed mounting bracket, and is mounted securely on the CNC machine table. The vector position of the workpiece relative to the CNC machine can be defined in the form of Machine Coordinate System (MCS). In Section 4.4, the customized tool path is defined as series of position vector of tool center points relative to the CCS. Tool path must be converted from CCS to MCS, which requires a homogeneous transformation matrix. In this section, two methods of coordinate registration will be introduced for different registration method in Section 4.3.

4.5.1 Coordinate Registration by Tooling Sphere

The coordinate registration will start with probing the tool spheres. The purpose of probing tool spheres is to locate the sphere center point vectors, $S_{x,MCS}$, $S_{y,MCS}$, $S_{z,MCS}$, relative to MCS. Herein, commonly used 5-hit method can be applied. First, probe the zenith (north pole) of the sphere and move the probe in negative z direction with the distance of sphere radius to the equator of sphere. Secondly, collect four sample points, from equator in X and Y axis, $S_{j,x}$ and $S_{j,y}$ respectively. The center point of each sphere is located by averaging the data of sample points in X and Y axis, respectively.

$$S_{x,MCS} = \frac{\sum_{j=1}^{M} S_{j,x}}{M} \tag{4.7}$$

$$S_{y,MCS} = \frac{\sum_{j=1}^{M} S_{j,y}}{M} \tag{4.8}$$

$$S_{z,MCS} = S_{j,z} - r \tag{4.9}$$

where M is the number of sphere sample points and r is the radius of sphere.

Alternatively, Orthogonal Least Squares Data Fitting method can be applied to acquire similar but more accurate value of sphere center point vectors. Detail of OLS can refer to Section 2.4.1. The sphere center points relative to MCS are then mapped to the corresponding points relative to CCS. The 4×4 $HTM_{CCS \to MCS}$ is then created to convert the customized tool path from CCS to MCS. As mentioned in Section 4.4, linked cutter contact points denote the tool path, and each point is presented as 1×3 matrix. For transformation purpose, 1×3 is represented as $i \times 4$ matrix form:

$P = \begin{bmatrix} X_i & Y_i & Z_i & 1 \end{bmatrix}$, where *i* indexes through the set of cutter center points.

4.5.2 Coordinate Registration by 3-2-1 Alignment

In Section 4.3.2, datum planes on the blade assembly were used for registration by 3-2-1 alignment method. In this section, datum planes on the workpiece will be used for coordinate registration to transform the coordinate system from MCS to CCS. Detailed description is listed in Section 2.4.2. Required points are determined by probing the datum planes with a touch-trigger probe as demonstrated in Figure 4.11, and then importing into commercial inspection software, Geomagic Qualify [49], for generating the 4×4 $HTM_{CCS \to MCS}$. Finally, the coordinate system of the customized tool path is transformed into MCS.

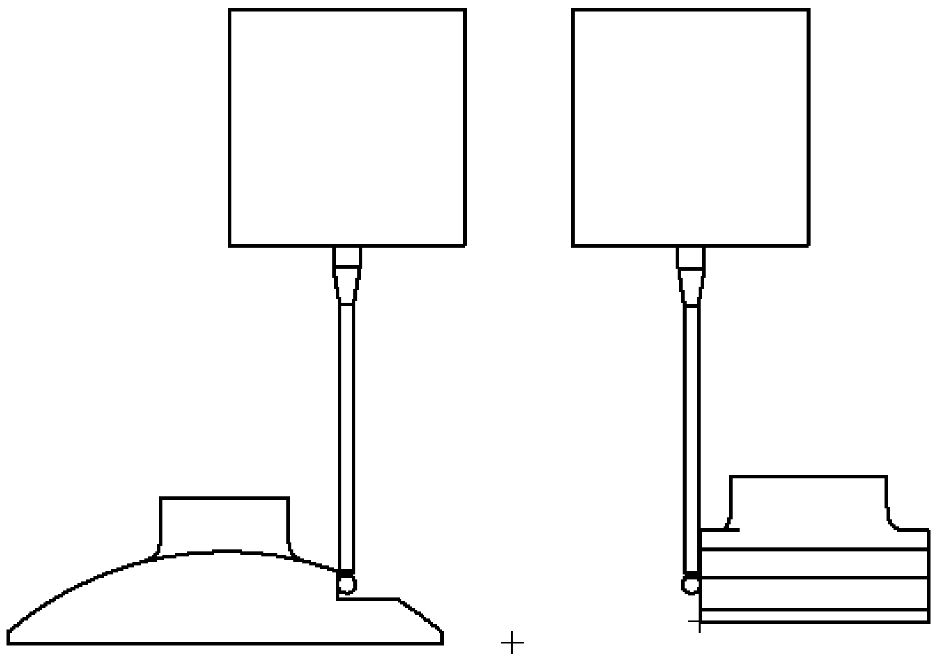

Figure 4.11. Coordinate registration by 3-2-1 alignment

4.6 CNC Machining

The CNC machining of blade assembly was validated on the McMaster Matsuura FX 5G/Fanuc 15i CNC three-axis CNC machine tool. The machine setup is presented in Figure 4.12 and 4.14, which includes simulated blade attached disk, fixture disk, and four 2-4-6 blocks. As mentioned before, this thesis work focuses on the flexibility of the proposed machining strategy, which can be adapted to blades from different vendors. Therefore, instead of selecting a particular vendor a CAD simulated blade-attached-disk is used. (See Appendix A.1 for drawing of the simulated blade-attached-disk.) Comparing to normal size fan blade shown in **Error! Reference source not found.**, the simulated lade-attached-disk has been scaled down for the purpose of strategy development. Since registration between workpiece and machine tool coordinate system is required, a fixture disk (see Appendix A.2 for drawing of the fixture disk) was designed for mounting workpiece and datum features.

Figure 4.12. Blade loaded into the fixture which is attached to table of the Matsuura FX 5G 3-axis machine tool

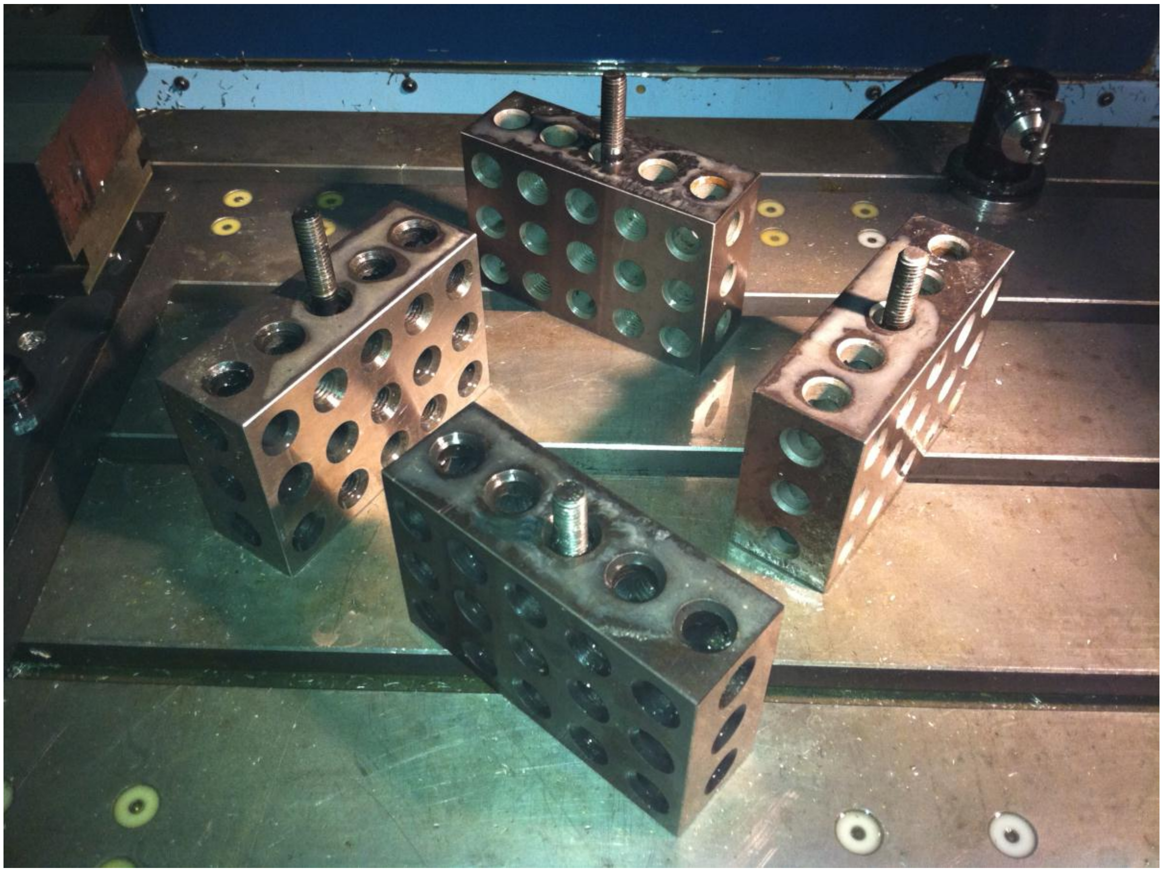

Figure 4.13. 2-4-6 blocks support of fixture for height adjustment

The customized tool path is loaded on controller and executed with an 8 mm diameter 2 flute ball nose end mill. As mentioned in Section 4.4, the uncut volumes of weld material are small. Good surface finish at the fillet zone can be achieved by using a cutter radius smaller than the fillet radius. The machining results will be discussed in the next chapter.

4.7 Summary

In this chapter, the workflow of rough machining excess weld material for joined blade assembly was discussed. During customization process, the dimensional difference between the actual blade assembly and the tool path can be pre-determined in the ACIS/HOOPS kernel to prevent gouging. After CNC machining, the joining edge can be grinded manually to produce flawless result. This method greatly improves the machining efficiency, accuracy and precision comparing to manual process.

Herein, helical downward tool path direction was presented for presentation purposes. The tool path direction can be adjusted to travel along the blade cross-sectional profile and step down incrementally. Tool lifting, re-entry and traveling distance can be minimized. This approach is similar to trochoidal milling, and allows better uncut chip thickness control than a path consisting of multiple passes around the whole fillet. It is easier to adjust along to actual geometry, and, when extended to 5-axis milling, will require much less rotary table motion.

The tool path algorithm can be directly applied to industrial scale fan blade assembly. Because the welding area of industrial scale fan blade only differs from the simulated blade assembly in one dimension, which is the blade contour, scale difference will not affect the final machining results. However, the rotary type laser scanner might not be the optimal choice of digitizing device due to the dimensional limitation. The laser digitizer integrated CNC machine tool configuration is preferred because of high resolution laser scanner and high positional accuracy AC servo motor implemented.

The tool path algorithm is also capable of machining excess weld material for different welding methods, such as linear friction welding. The welding area of blade joined by linear friction welding is typically located at blade surface near shaft. Therefore, the surface continuity replies on two freeform surfaces, the blade surfaces above and below the joining area. Other than blade assembly machining, the refurbishment of mould can also adapt the proposed machining workflow.

Chapter 5

Machining Results

The machining strategy proposed in this thesis was validated in three stages. For process development, the initial validation was performed on the cylinder assembly presented in Section 5.1. Next the machining process was adapted for simulated blade assembly, where the blade was at nominal position as presented in Section 5.2. Finally, the machining process was tested on two offset blade assemblies as presented in Section 5.3.

5.1 Cylinder Assembly Machining

The machining result for the cylinder assembly is presented in Figure 5.2. The majority of the excess weld material was successfully removed. The customized tool path that was constructed based solely on the fillet radius did not include adjacent surfaces on the blade and hub/shaft. Because of inconsistent welding, material could extend onto the blade and hub/shaft surface. To solve this issue, the customized tool path will be further extended in subsequent machining tests.

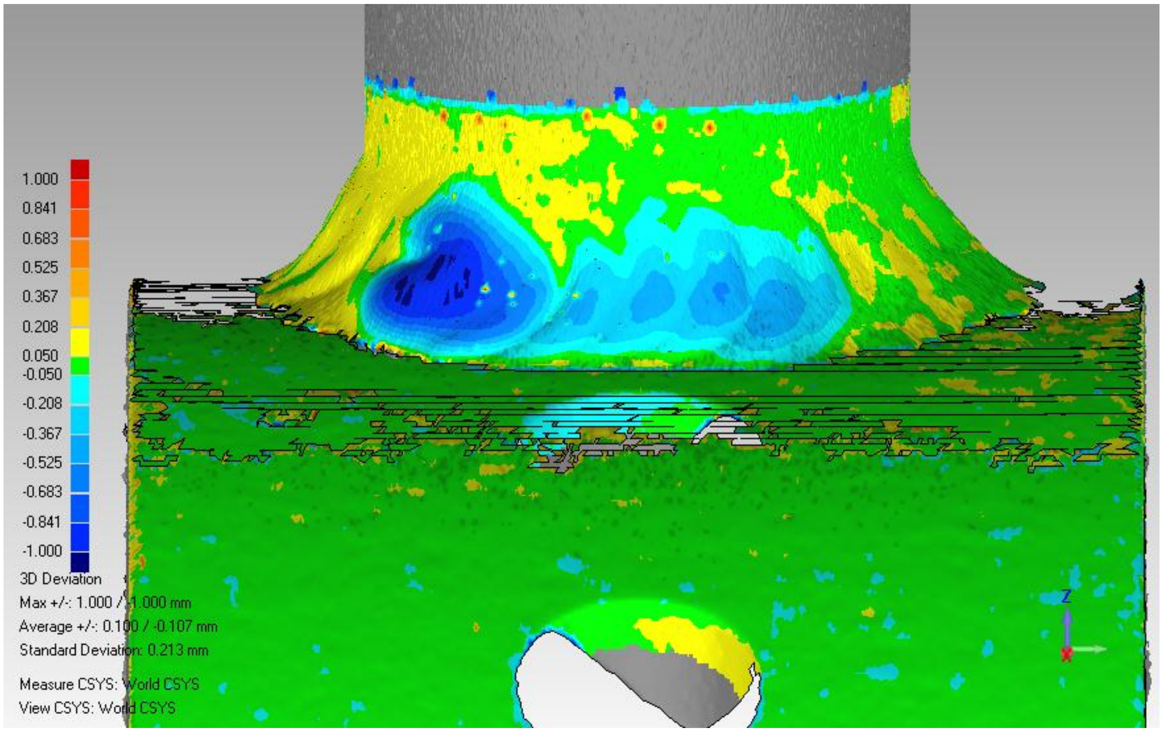

Figure 5.1. Comparison of cylinder assembly before/after machining

Figure 5.2. Photograph of a refurbished cylinder assembly

5.2 Nominal Blade Assembly Machining

In this section, the simulated assembly, with the blade at its nominal position is machined, with the extended and customized tool path. The purpose of this machining experiment is to validate the customized tool path. The machining result is presented in Figure 5.3 and Figure 5.4. In order to validate the transition surface smoothness, the machined blade assembly is digitized and compared with the reference geometry blade assembly (Figure 5.3). The machined area (circled in Figure 5.3) has a relatively small dimensional difference (less than 0.5 mm).

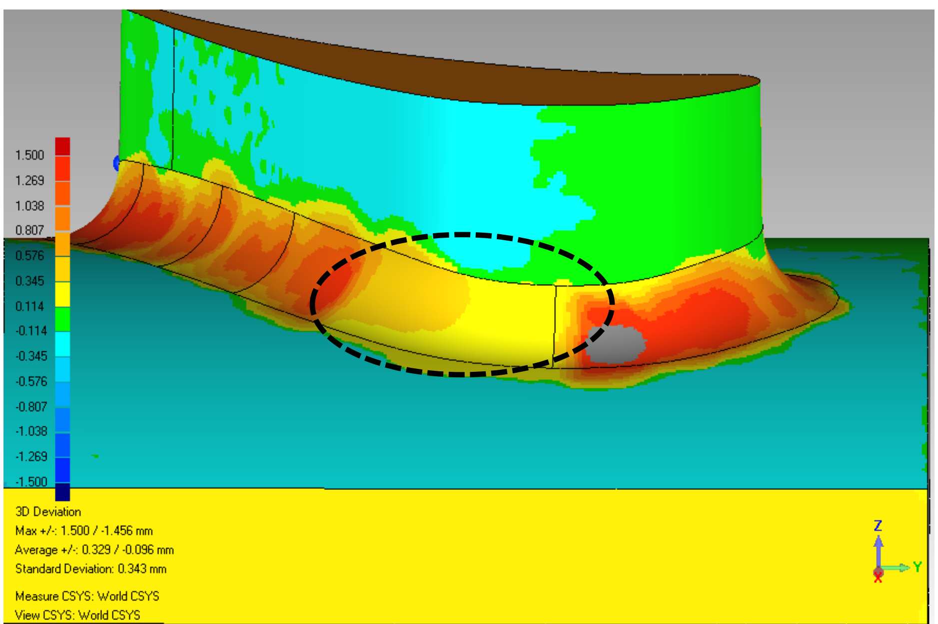

Figure 5.3. Comparison of welded and machined to reference geometry (precisely positioned blade assembly)

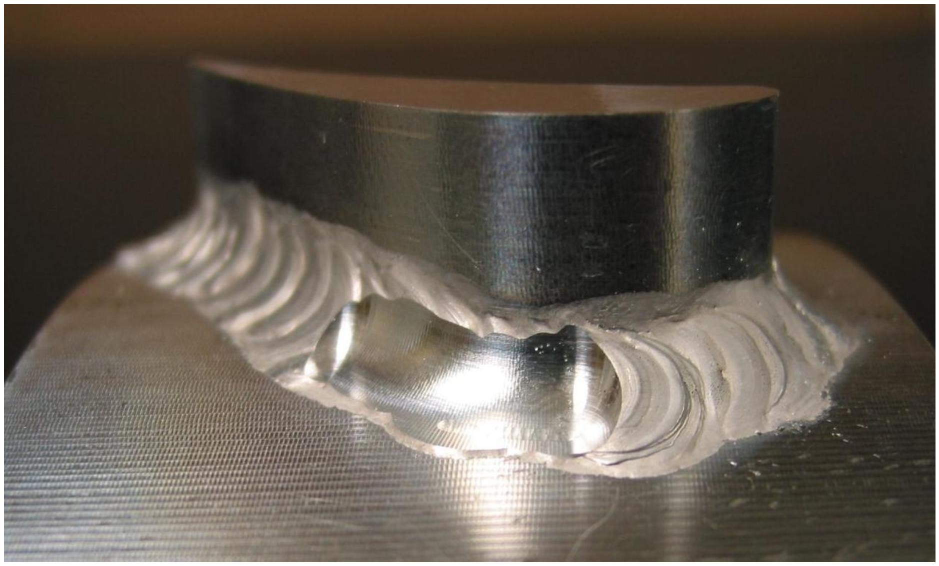

Figure 5.4. Photograph of welded and machined result (precisely positioned blade assembly)

5.3 Offset Blade Assembly Machining

In this section, two experiments are performed in order to validate the machining process with a misaligned blade assembly. To simulate the misalignment, the blade position is shifted in translational and rotational directions. Figure 5.5 illustrates the cross-sectional comparison between a misaligned blade (presented by dashed line) and a precisely positioned blade (presented by solid line). The tables followed by the machining results contain the average value of blade and shaft misalignment, which provides “go/no go” indication before machining.

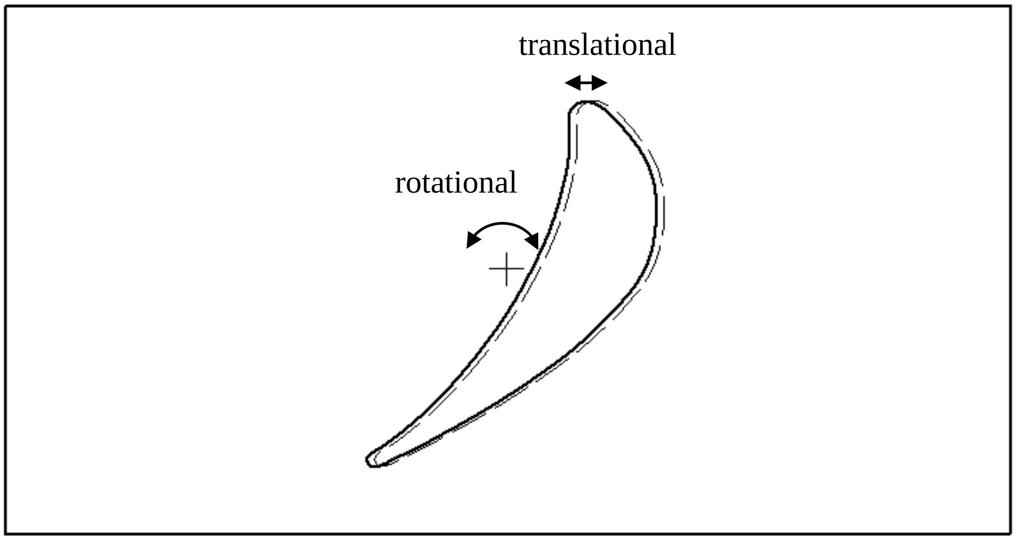

Figure 5.5. Schematic diagram of blade assembly misalignment

5.3.1 Offset by Negative 0.5 mm and 1^{o} Clockwise

Herein, the misalignment of the blade position is negative 0.5 mm in the translational direction and 1^{o} clockwise in the rotational direction as shown in Figure 5.6. The blade/fillet and shaft/fillet joints are compared with the reference geometry in Figure 5.7. The machining result is presented in Figure 5.8 and Figure 5.9. As seen in the circled area of Figure 5.8, the customized tool path results in smooth transition across the fillet with less than 0.5 mm dimensional error.

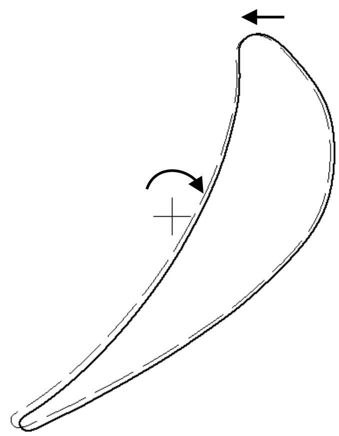

Figure 5.6. Blade assembly misaligned by negative 0.5 mm and 1^{o} clockwise

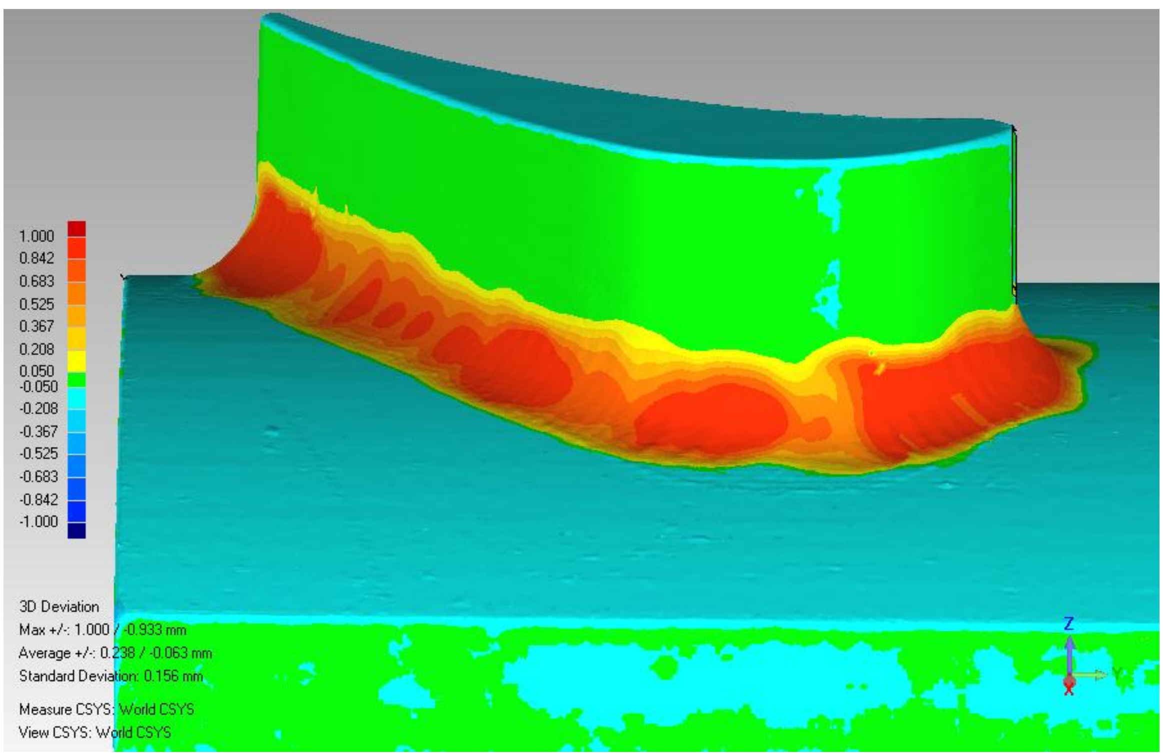

Figure 5.7. Comparison of welded and reference geometry misaligned blade assembly for the case of negative 0.5 mm and 1^{o} clockwise (before machining)

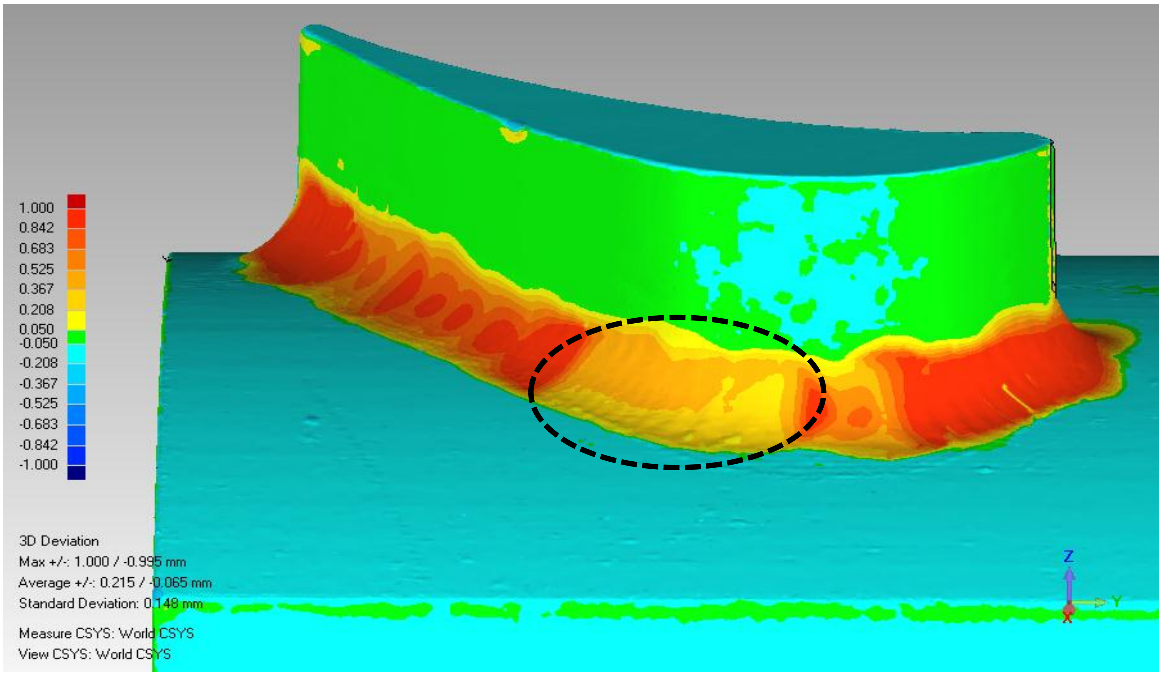

Figure 5.8. Comparison of welded and reference geometry misaligned blade assembly for the case of negative 0.5 mm and 1^{o} clockwise (after machining)

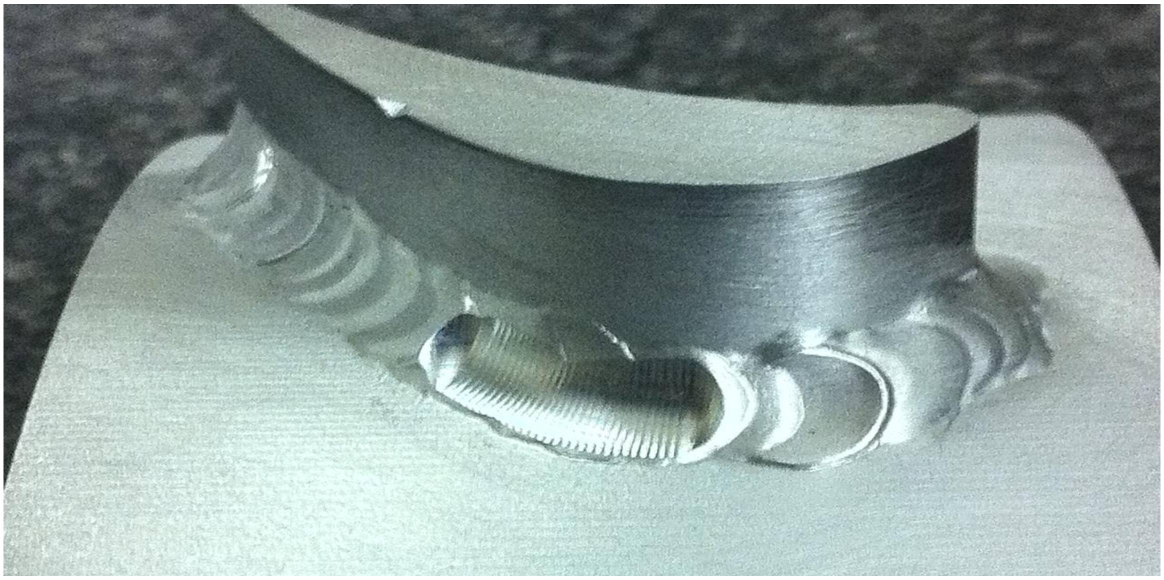

Figure 5.9 Photograph of a machined misaligned blade assembly for the case of negative 0.5 mm and 1^{o} clockwise

Case: -0.5 mm and 1 degree clockwise											
Loop Number	Blade Offset (mm)										
	1	2	3	4	5	6	7	8	9	10	Average
1	-0.605	-0.601	-0.600	-0.603	-0.608	-0.611	-0.615	-0.619	-0.619	-0.614	-0.609
2	-0.604	-0.600	-0.598	-0.603	-0.609	-0.614	-0.618	-0.620	-0.616	-0.609	-0.609
3	-0.604	-0.602	-0.600	-0.604	-0.611	-0.615	-0.618	-0.619	-0.616	-0.607	-0.610
4	-0.605	-0.603	-0.603	-0.607	-0.611	-0.615	-0.619	-0.618	-0.614	-0.610	-0.611
5	-0.606	-0.606	-0.606	-0.610	-0.611	-0.614	-0.619	-0.620	-0.616	-0.615	-0.612
6	-0.606	-0.608	-0.609	-0.611	-0.612	-0.613	-0.619	-0.623	-0.621	-0.620	-0.614
7	-0.606	-0.607	-0.609	-0.610	-0.610	-0.614	-0.621	-0.625	-0.625	-0.624	-0.615
8	-0.602	-0.604	-0.606	-0.608	-0.611	-0.615	-0.621	-0.624	-0.625	-0.625	-0.614
9	-0.596	-0.598	-0.602	-0.605	-0.608	-0.612	-0.619	-0.622	-0.623	-0.623	-0.611
10	-0.585	-0.590	-0.595	-0.600	-0.604	-0.608	-0.612	-0.616	-0.618	-0.617	-0.604
11	-0.573	-0.581	-0.586	-0.593	-0.598	-0.600	-0.603	-0.606	-0.608	-0.608	-0.595
12	-0.561	-0.571	-0.577	-0.585	-0.590	-0.591	-0.589	-0.593	-0.597	-0.598	-0.585
13	-0.549	-0.559	-0.569	-0.575	-0.579	-0.579	-0.576	-0.579	-0.586	-0.587	-0.574
14	-0.539	-0.548	-0.558	-0.566	-0.567	-0.568	-0.564	-0.570	-0.576	-0.577	-0.563
15	-0.531	-0.537	-0.546	-0.554	-0.557	-0.556	-0.553	-0.559	-0.567	-0.568	-0.553
16	-0.520	-0.526	-0.535	-0.545	-0.547	-0.546	-0.543	-0.553	-0.558	-0.556	-0.543
17	-0.508	-0.513	-0.523	-0.534	-0.537	-0.538	-0.536	-0.542	-0.547	-0.545	-0.532
18	-0.494	-0.497	-0.512	-0.525	-0.528	-0.529	-0.530	-0.534	-0.534	-0.530	-0.521
19	-0.478	-0.482	-0.498	-0.511	-0.517	-0.522	-0.522	-0.522	-0.520	-0.518	-0.509
20	-0.464	-0.468	-0.483	-0.495	-0.505	-0.510	-0.510	-0.507	-0.504	-0.504	-0.495
21	-0.452	-0.456	-0.467	-0.478	-0.488	-0.494	-0.494	-0.491	-0.488	-0.491	-0.480
22	-0.439	-0.443	-0.452	-0.460	-0.470	-0.475	-0.475	-0.474	-0.471	-0.474	-0.463
23	-0.430	-0.435	-0.438	-0.443	-0.452	-0.456	-0.458	-0.458	-0.456	-0.458	-0.448
24	-0.423	-0.426	-0.426	-0.429	-0.436	-0.438	-0.441	-0.446	-0.444	-0.444	-0.435
25	-0.417	-0.419	-0.417	-0.420	-0.421	-0.422	-0.427	-0.433	-0.435	-0.432	-0.424
26	-0.413	-0.414	-0.412	-0.412	-0.414	-0.413	-0.417	-0.425	-0.428	-0.430	-0.418
27	-0.412	-0.411	-0.408	-0.407	-0.408	-0.408	-0.412	-0.421	-0.426	-0.429	-0.414
28	-0.411	-0.411	-0.408	-0.405	-0.406	-0.409	-0.414	-0.421	-0.425	-0.428	-0.414
29	-0.411	-0.410	-0.407	-0.403	-0.403	-0.408	-0.414	-0.419	-0.424	-0.424	-0.412
30	-0.411	-0.410	-0.405	-0.401	-0.402	-0.405	-0.412	-0.417	-0.420	-0.423	-0.411
31	-0.411	-0.408	-0.404	-0.399	-0.399	-0.403	-0.409	-0.414	-0.417	-0.419	-0.408
32	-0.409	-0.407	-0.402	-0.397	-0.396	-0.400	-0.405	-0.410	-0.412	-0.413	-0.405

Table 5.1. Offset at blade for the case of negative 0.5 mm and 1^{o} clockwise

Case: -0.5 mm and 1 degree clockwise											
Loop Number	Shaft Offset (mm)										
	1	2	3	4	5	6	7	8	9	10	Average
1	0.108	0.099	0.091	0.084	0.083	0.087	0.092	0.097	0.099	0.098	0.094
2	0.112	0.101	0.092	0.087	0.086	0.090	0.094	0.098	0.099	0.099	0.096
3	0.114	0.102	0.093	0.089	0.089	0.092	0.095	0.098	0.100	0.099	0.097
4	0.113	0.101	0.093	0.090	0.090	0.093	0.096	0.099	0.124	0.098	0.100
5	0.111	0.101	0.092	0.092	0.092	0.094	0.097	0.099	0.100	0.098	0.098
6	0.108	0.100	0.093	0.092	0.093	0.096	0.098	0.101	0.100	0.099	0.098
7	0.101	0.096	0.092	0.093	0.094	0.097	0.101	0.102	0.102	0.100	0.098
8	0.096	0.091	0.090	0.092	0.096	0.099	0.103	0.104	0.104	0.102	0.098
9	0.094	0.089	0.089	0.092	0.096	0.101	0.104	0.106	0.105	0.103	0.098
10	0.096	0.090	0.091	0.094	0.098	0.102	0.106	0.107	0.106	0.104	0.099
11	0.100	0.096	0.095	0.098	0.102	0.106	0.108	0.108	0.107	0.104	0.102
12	0.106	0.102	0.101	0.104	0.108	0.110	0.111	0.109	0.107	0.105	0.106
13	0.107	0.106	0.107	0.110	0.113	0.114	0.113	0.112	0.109	0.107	0.110
14	0.107	0.108	0.111	0.114	0.117	0.117	0.115	0.114	0.110	0.108	0.112
15	0.108	0.111	0.114	0.117	0.120	0.119	0.117	0.114	0.112	0.109	0.114
16	0.110	0.114	0.117	0.119	0.121	0.120	0.117	0.114	0.112	0.110	0.115
17	0.112	0.115	0.118	0.119	0.119	0.118	0.117	0.113	0.111	0.109	0.115
18	0.114	0.117	0.119	0.119	0.119	0.117	0.114	0.112	0.111	0.110	0.115
19	0.117	0.119	0.121	0.120	0.118	0.117	0.115	0.113	0.111	0.109	0.116
20	0.120	0.123	0.123	0.021	0.119	0.119	0.117	0.114	0.112	0.111	0.108
21	0.122	0.125	0.124	0.123	0.122	0.121	0.119	0.116	0.114	0.111	0.120
22	0.124	0.125	0.124	0.123	0.123	0.121	0.119	0.118	0.116	0.113	0.121
23	0.124	0.124	0.123	0.123	0.123	0.122	0.121	0.120	0.118	0.115	0.121
24	0.123	0.122	0.122	0.122	0.122	0.123	0.122	0.122	0.120	0.118	0.122
25	0.121	0.120	0.122	0.123	0.124	0.124	0.125	0.123	0.122	0.120	0.122
26	0.118	0.119	0.122	0.125	0.127	0.128	0.127	0.125	0.124	0.122	0.124
27	0.117	0.118	0.123	0.127	0.130	0.130	0.130	0.129	0.126	0.124	0.125
28	0.117	0.120	0.125	0.130	0.132	0.133	0.134	0.132	0.129	0.126	0.128
29	0.122	0.125	0.129	0.133	0.135	0.136	0.135	0.134	0.131	0.127	0.131
30	0.128	0.130	0.134	0.136	0.137	0.138	0.137	0.135	0.132	0.128	0.134
31	0.133	0.135	0.137	0.138	0.140	0.141	0.139	0.135	0.132	0.128	0.136
32	0.137	0.139	0.140	0.140	0.142	0.142	0.138	0.136	0.132	0.130	0.137

Table 5.2. Offset at shaft for the case of negative 0.5 mm and 1^o clockwise

5.3.2 Offset by Positive 0.5 mm and 1^o Counter-clockwise

In this section, the direction of blade misalignment is inversed, where the blade position is shifted in positive 0.5 mm and rotated in 1^o counter-clockwise as seen in Figure 5.10. Figure 5.12 to Figure 5.13 illustrates the result. A smooth surface finish with less than 0.5 mm dimensional error was achieved.

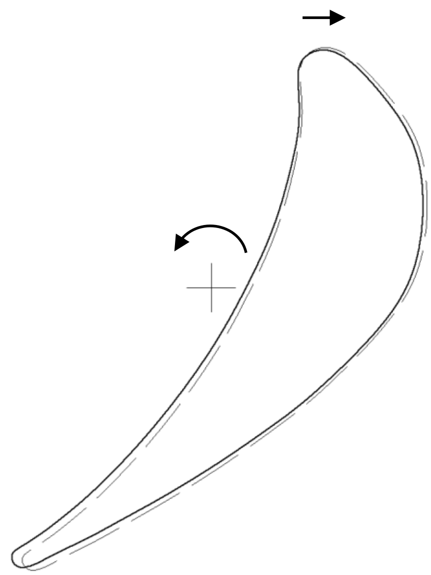

Figure 5.10. Blade assembly misaligned by positive 0.5 mm and 1^{o} counter-clockwise

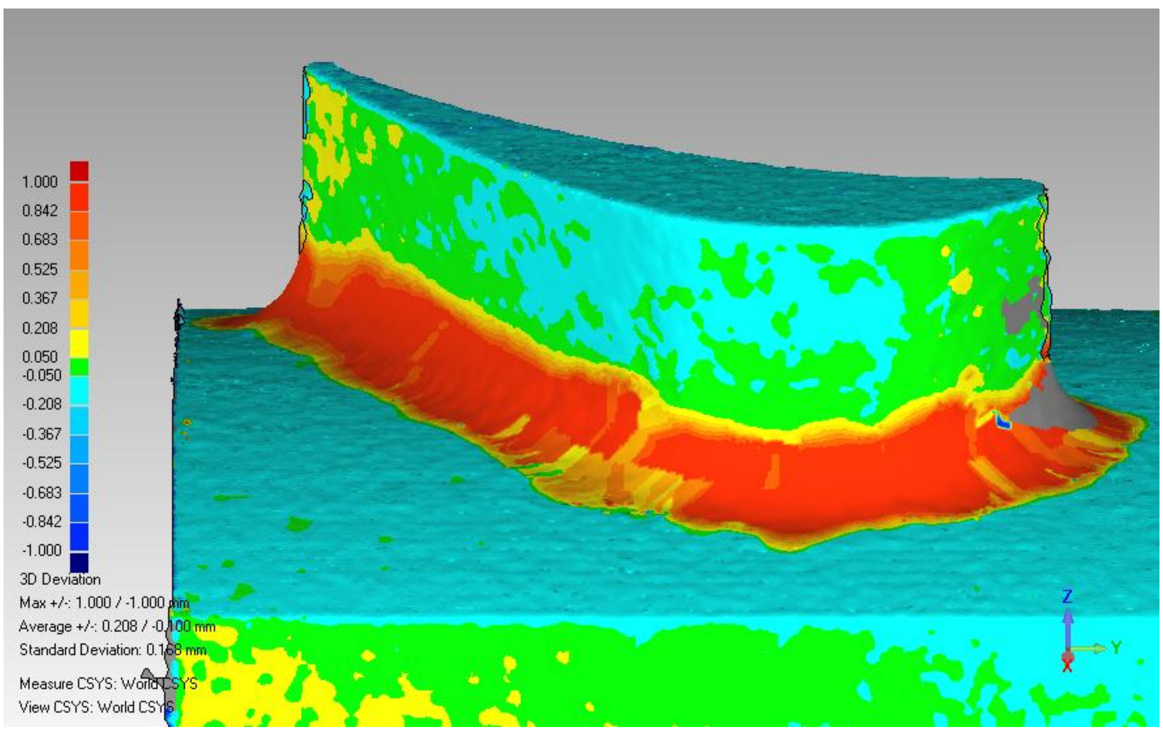

Figure 5.11. Comparison of welded and reference geometry misaligned blade assembly for the case of positive 0.5 mm and 1^{o} counter-clockwise (before machining)

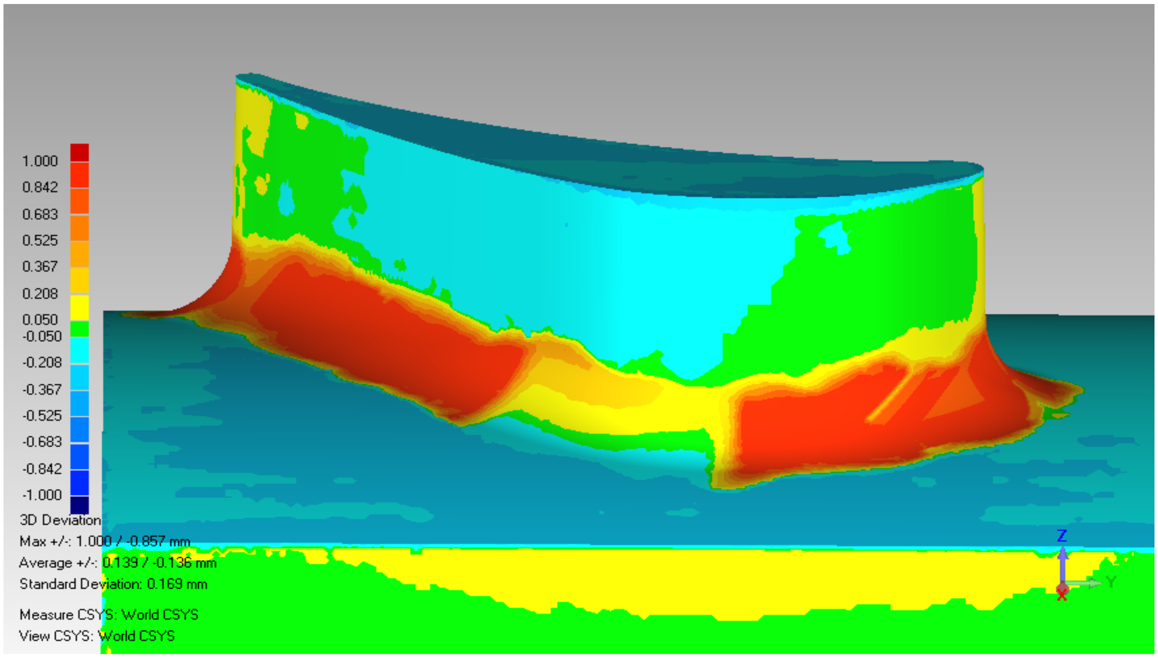

Figure 5.12. Comparison of welded and reference geometry misaligned blade assembly for the case of positive 0.5 mm and 1^{o} counter-clockwise (after machining)

Figure 5.13. Photograph of a refurbished misaligned blade assembly for the case of positive 0.5 mm and 1^{o} counter-clockwise

Case: +0.5 mm and 1 degree counter-clockwise											
Loop	Blade Offset (mm)										
Number	1	2	3	4	5	6	7	8	9	10	Average
1	0.284	0.295	0.293	0.307	0.299	0.329	0.314	0.289	0.282	0.291	0.298
2	0.287	0.300	0.288	0.303	0.288	0.318	0.329	0.288	0.282	0.287	0.297
3	0.286	0.302	0.279	0.293	0.281	0.299	0.321	0.293	0.292	0.282	0.293
4	0.281	0.307	0.271	0.283	0.279	0.286	0.295	0.294	0.301	0.296	0.289
5	0.276	0.306	0.269	0.280	0.275	0.288	0.289	0.289	0.300	0.306	0.288
6	0.276	0.301	0.272	0.294	0.266	0.279	0.287	0.282	0.285	0.291	0.283
7	0.274	0.289	0.277	0.295	0.251	0.261	0.281	0.283	0.280	0.278	0.277
8	0.264	0.272	0.286	0.286	0.245	0.256	0.275	0.282	0.281	0.278	0.273
9	0.259	0.283	0.293	0.277	0.253	0.256	0.261	0.269	0.283	0.291	0.272
10	0.257	0.298	0.300	0.269	0.272	0.267	0.255	0.260	0.285	0.311	0.277
11	0.252	0.299	0.311	0.263	0.279	0.285	0.255	0.264	0.285	0.316	0.281
12	0.240	0.285	0.306	0.255	0.268	0.287	0.258	0.268	0.280	0.307	0.276
13	0.233	0.270	0.286	0.254	0.255	0.271	0.267	0.270	0.264	0.273	0.264
14	0.239	0.260	0.268	0.255	0.241	0.247	0.251	0.260	0.247	0.250	0.252
15	0.245	0.245	0.265	0.256	0.238	0.227	0.233	0.262	0.247	0.242	0.246
16	0.238	0.235	0.261	0.251	0.245	0.224	0.227	0.269	0.257	0.239	0.245
17	0.226	0.228	0.258	0.245	0.249	0.228	0.226	0.265	0.253	0.233	0.241
18	0.216	0.224	0.249	0.232	0.246	0.234	0.231	0.249	0.243	0.234	0.236
19	0.211	0.229	0.241	0.225	0.235	0.234	0.244	0.241	0.228	0.230	0.232
20	0.214	0.235	0.234	0.226	0.223	0.229	0.247	0.227	0.218	0.223	0.227
21	0.226	0.235	0.229	0.223	0.215	0.218	0.238	0.221	0.220	0.219	0.225
22	0.233	0.229	0.223	0.211	0.208	0.212	0.223	0.219	0.216	0.213	0.219
23	0.218	0.220	0.209	0.200	0.209	0.210	0.213	0.208	0.197	0.197	0.208
24	0.204	0.211	0.198	0.204	0.225	0.214	0.214	0.201	0.195	0.189	0.205
25	0.206	0.201	0.191	0.203	0.225	0.209	0.197	0.203	0.195	0.182	0.201
26	0.210	0.197	0.194	0.192	0.202	0.195	0.173	0.187	0.190	0.169	0.191
27	0.204	0.192	0.189	0.186	0.180	0.190	0.157	0.154	0.173	0.164	0.179
28	0.190	0.188	0.176	0.189	0.183	0.187	0.152	0.147	0.171	0.167	0.175
29	0.175	0.190	0.183	0.193	0.185	0.171	0.154	0.154	0.172	0.175	0.175
30	0.172	0.189	0.204	0.181	0.175	0.162	0.155	0.157	0.163	0.174	0.173
31	0.177	0.190	0.216	0.173	0.167	0.173	0.161	0.160	0.165	0.178	0.176
32	0.191	0.203	0.223	0.193	0.186	0.191	0.169	0.168	0.176	0.189	0.189

Table 5.3. Offset at blade for the case of positive 0.5 mm and 1^{o} counter-clockwise

Case: +0.5 mm and 1 degree counter-clockwise											
Loop Number	Shaft Offset (mm)										
	1	2	3	4	5	6	7	8	9	10	Average
1	0.005	0.020	0.019	0.022	0.022	0.015	0.023	0.038	0.026	0.013	0.020
2	0.020	0.017	0.027	0.027	0.028	0.019	0.027	0.042	0.031	0.019	0.026
3	0.000	0.016	0.023	0.035	0.032	0.025	0.025	0.027	0.018	0.022	0.022
4	0.006	0.013	0.029	0.037	0.030	0.035	0.038	0.021	0.014	0.027	0.025
5	0.001	0.015	0.035	0.033	0.020	0.030	0.030	0.013	0.020	0.033	0.023
6	0.023	0.022	0.033	0.045	0.033	0.032	0.034	0.021	0.025	0.027	0.029
7	0.012	0.019	0.033	0.054	0.063	0.055	0.041	0.030	0.027	0.018	0.035
8	0.019	0.022	0.028	0.043	0.057	0.043	0.026	0.029	0.035	0.027	0.033
9	0.030	0.034	0.024	0.034	0.047	0.032	0.022	0.027	0.035	0.040	0.033
10	0.050	0.052	0.040	0.040	0.046	0.045	0.041	0.043	0.042	0.042	0.044
11	0.057	0.063	0.057	0.044	0.041	0.050	0.045	0.034	0.035	0.043	0.047
12	0.040	0.051	0.059	0.063	0.039	0.018	0.013	0.018	0.030	0.046	0.038
13	0.036	0.041	0.046	0.049	0.030	0.018	0.025	0.032	0.046	0.055	0.038
14	0.044	0.037	0.030	0.030	0.026	0.044	0.056	0.055	0.059	0.054	0.044
15	0.037	0.023	0.012	0.018	0.034	0.056	0.054	0.061	0.080	0.068	0.044
16	0.026	0.011	0.009	0.022	0.044	0.051	0.038	0.045	0.067	0.065	0.038
17	0.033	0.016	0.010	0.024	0.046	0.048	0.028	0.034	0.038	0.037	0.031
18	0.043	0.031	0.022	0.024	0.030	0.031	0.033	0.041	0.037	0.026	0.032
19	0.034	0.031	0.030	0.028	0.027	0.036	0.049	0.057	0.043	0.029	0.036
20	0.027	0.021	0.023	0.033	0.037	0.049	0.058	0.073	0.046	0.037	0.040
21	0.007	0.006	0.016	0.022	0.034	0.057	0.067	0.069	0.042	0.044	0.036
22	0.007	0.008	0.017	0.030	0.055	0.071	0.064	0.057	0.046	0.046	0.040
23	0.013	0.023	0.038	0.058	0.073	0.072	0.059	0.045	0.028	0.030	0.044
24	0.024	0.030	0.049	0.065	0.068	0.066	0.061	0.049	0.032	0.025	0.047
25	0.035	0.038	0.048	0.064	0.071	0.069	0.067	0.052	0.047	0.043	0.053
26	0.050	0.038	0.046	0.066	0.074	0.069	0.058	0.036	0.040	0.043	0.052
27	0.064	0.044	0.050	0.048	0.045	0.047	0.036	0.026	0.027	0.029	0.042
28	0.074	0.067	0.057	0.040	0.032	0.038	0.035	0.028	0.026	0.032	0.043
29	0.067	0.079	0.060	0.046	0.039	0.033	0.027	0.028	0.032	0.036	0.045
30	0.058	0.051	0.042	0.040	0.041	0.027	0.026	0.043	0.049	0.043	0.042
31	0.045	0.039	0.037	0.039	0.044	0.027	0.032	0.053	0.055	0.046	0.042
32	0.022	0.029	0.038	0.053	0.065	0.040	0.040	0.052	0.049	0.039	0.043

Table 5.4. Offset at shaft for the case of positive 0.5 mm and 1^{o} counter-clockwise

5.4 Uncertainties and Safety Margin

The workflow introduced herein can improve the efficiency and precision of post-process machining of excess weld material as compared to a conventional manual process. To account for known errors in the system a safety margin is applied to keep from gouging the blade or shaft surface. Gouging of the surface must be prevented during the machining process to avoid scrapping the blade. The safety margin was established based on an estimate of the known errors in the system. Table 5.5 provides an estimate of the maximum value of error that can occur with the major system elements. These values are established based on the industry standards as discussed further in the next paragraph.

Uncertainty Factors	Value
Magnaflux SDK Developer	0.135 mm
Roland LPX-600 Laser Scanner	0.05 mm
Renishaw MP12 Probe System	0.04 mm
Cutting Tool	0.06 mm (tool dependant)
Safety Margin	0.08 mm (user controlled)
CNC Machining	0.01 mm
Relative Tool – Workpiece Deflection	-0.007 mm (not included at this stage)
Geomagic	<0.001 mm
Total	0.375 mm

Table 5.5. Uncertainty factors and safety margin

During laser scanning process, the Magnaflux SDK developer [44] creates a layer of uneven surface coating with thickness of approximately 0.078 mm. The coating thickness is estimated by the coverage area (65 square feet) of a 16 oz. aerosol can [50]. The surface of the welded blade assembly is expected to create an additional thickness of 0.078 mm. During the 3-2-1 registration by Geomagic, the alignment of datum planes YZ, XZ and XY as seen from Figure 5.14 translated the welded blade assembly by -0.078 mm in X axis, +0.078 mm in Y axis and -0.078 mm in Z axis respectively. This resulted in the uncertainty range of -0.015 mm to -0.135 mm at blade suction side and +0.035 mm to –0.095 mm at blade pressure side as seen in Figure 5.15. The developer error accounts for the major uncertainty.

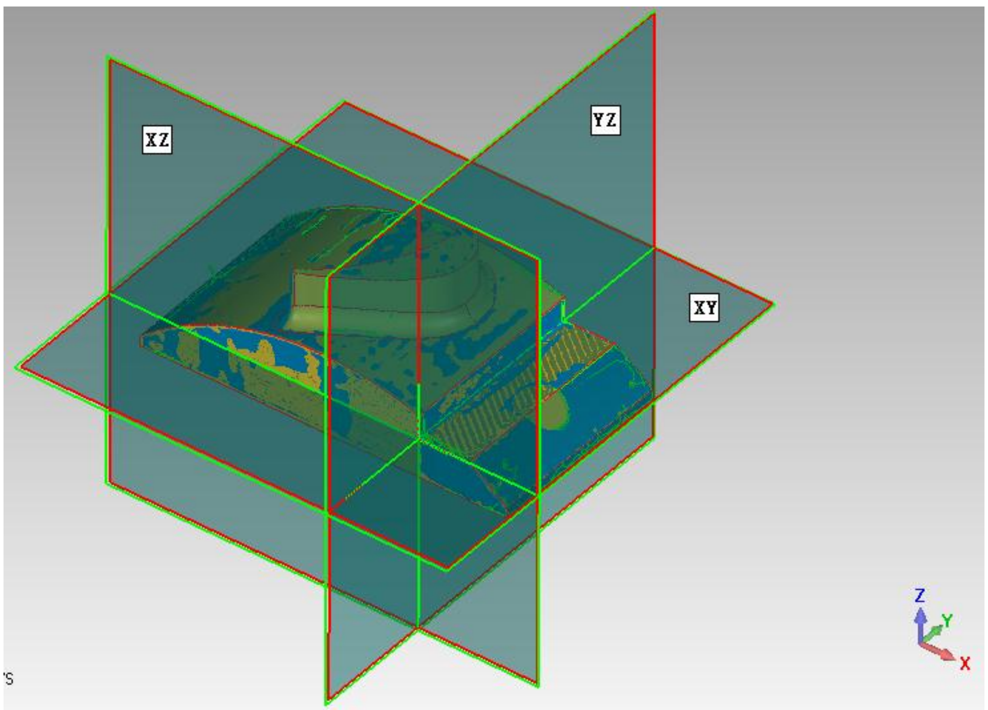

Figure 5.14. 3-2-1 registration datum planes: XZ, YZ and XY

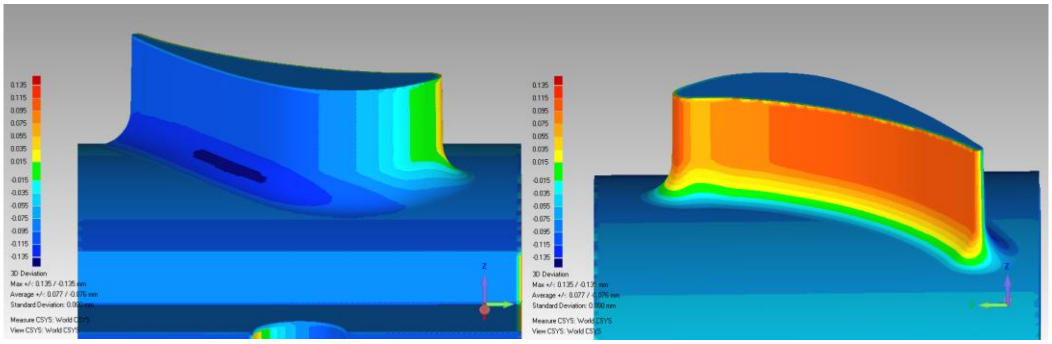

(a) (b)

Figure 5.15. Range of uncertainty caused by developer coating: (a) blade suction side; (b) blade pressure side

Other factors are categorized as equipment uncertainties, including laser scanning accuracy, probe system pre-travel, cutting tool runout, and CNC machine tool accuracy. The Roland LPX-600 laser scanner [22] has a 0.05 mm system uncertainty based on the equipment specification provided by manufacturer. The Renishaw M12 probe system [17] has a directional pre-travel variation from 0.05 mm to 0.09 mm, which results in 0.04 mm measuring uncertainty. The pre-travel error is estimated through multiple ring gouge calibration experiments. The difference between the measured cutter diameter (7.88 mm) and the cutter diameter (8.00 mm) used to generate the customized tool path was 0.12 mm diameter or 0.06 radius runout. This contributed to an increase in the margin. In the future the actual tool should be measured before developing the tool path. Altering the effective tool diameter is how the margin was implemented in this case. A well maintained and regularly calibrated 3-axis CNC machine tool is expected to have a value of 0.01 mm based on the past machining experiences of Matsuura FX-5G 3-axis machine tool. Detailed testing would need to be performed for a 5-axis machine to establish a realistic value.

The remaining factors are categorized as assumed uncertainties, including relative tool – workpiece deflection and Geomagic software error. Because down milling is implemented, the tool deflection due to cutting forces will be almost perpendicular to the cut, which leads to slight tool deflection in the direction away from the part as illustrated in Figure 5.16 and negative uncertainty value of relative tool – workpiece deflection is expected. The tool tip deflection, δ_{tool}, can be calculated based on the estimated cutting force, F_{cut}, using the following equation in which the tool is considered as a cylindrical cantilever beam.

$$\delta_{tool} = \frac{F_{cut} \cdot L^3}{3 \cdot E_{tool} \cdot I} \tag{5.1}$$

where L is the protruding length of tool from the tool holder (30 mm), E is the Young's modulus of the tool (55000 N/mm^2), $I = \frac{D^4}{64}$ is the cross-sectional moment of inertia of a solid cylinder of the same diameter D [51]. The resulting equation is

$$\delta_{tool} = \frac{64 F_{cut} \cdot L^3}{3\pi \cdot E_{tool} \cdot D^4} \tag{5.2}$$

The maximum cutting force is estimated using the following equation [52].

$$F_{cut} = k_c \cdot b \cdot t \tag{5.3}$$

where k_c is the specific cutting force for 6061 aluminum alloy (450 N/mm^2), b is the chip load for a 8 mm diameter cutter (0.051 mm) and t is the depth of cut measured

(3.350 mm). The estimated cutting force is 76.883 N, which will lead to a relative tool – workpiece deflection of approximately 0.007 mm based on equation (5.2). Since the deflection is in the direction away from the workpiece, it should not be included at this stage to avoid a dwell mark at zero feed rate. Due to the uneven and unknown thickness of the weld bead, the actual value of tool – workpiece deflection is uncertain for each blade assembly. Therefore, a conservative safety margin of 0.08 mm was assigned to the tool path to ensure gouging avoidance. The value of safety margin could be further reduced based on the calculated tool – workpiece deflection of individual blade assembly. Detailed calculation could be included in the future with the implementation of a 5-axis machine and the reader is referred to [51], [52] and [53]. The mathematical fitting error of Geomagic is also assumed to be near zero, which requires further testing to establish a realistic value. All factors discussed account for the total estimated value of 0.375 mm.

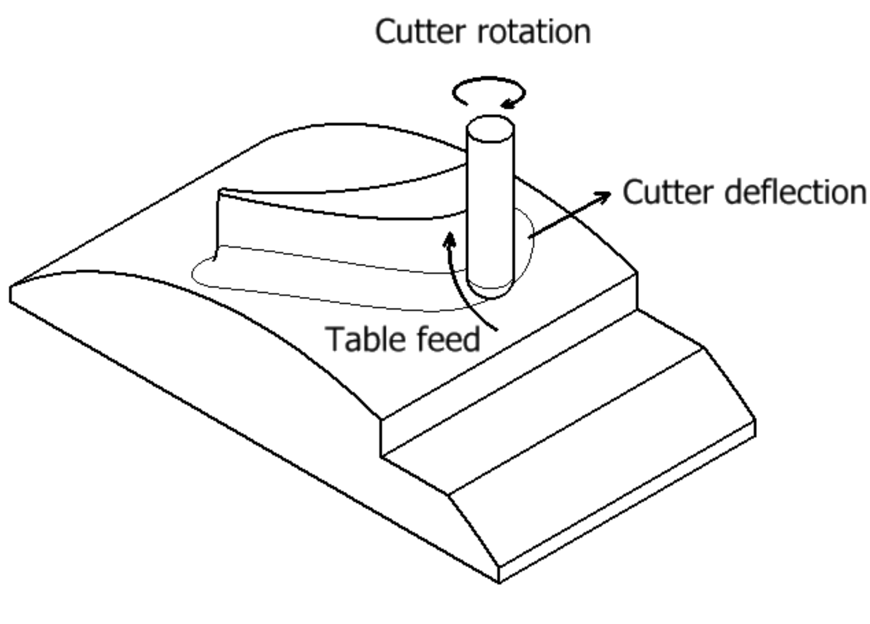

Figure 5.16. Direction of cutter deflection is away from the part for down milling

As seen from the machining results shown above, a thin layer of weld material with thickness of approximately 0.208 mm to 0.367 mm is still apparent on the part. This range for the excess material is very closed to the estimated value of the error expected and hence the safety margin left on the part is excessive and the value could be reduced in future refinements of the machining process. This step would require extensive experimentation to establish their error values when the system is fully implemented. Even with a safety margin still present on the surfaces the smoothness of the machined surface and its adherence to the desired shape represents significant value to the final manual polishing process as it allows the people doing the blending to hand finish to a precise reference surface. This will reduce the complexity of their job and allow them to perform their work more accurately resulting in higher quality parts.

Chapter 6

Conclusion and Future Works

A new joined blade measurement and machining system for finishing blade assembly fillets. The implemented workflow achieved the objectives outlined in the introduction of the thesis, which solved the part-to-part variation of joined fan blades. Integrated laser digitizing and CNC machining were applied to achieve the essential principle of automation and flexibility.

Following the procedures of the workflow, the surface geometry of joined blade was captured by the laser digitizer and constructed as a triangular facet mesh. The offset between the nominal and the actual blade position was extracted by projecting the nominal tool path onto the registered triangular model of actual blade. The tool path was then customized based on the previously determined offset following the author defined NURBS or interpolation algorithm in a CAD/CAM kernel. The CNC controller executed the customized tool path to eliminate surplus welding material.

The implemented workflow was verified on a three-axis machine tool by machining results, including two distinct blade samples. These initial results demonstrated the accuracy and repeatability of the joined blade refurbishment system.

6.1 Suggested Future Work

This thesis work has presented the system design for joined blade measurement and refurbishing, and has contributed an algorithm for three-axis tool path customization. Future development will move toward the industrial blade design, which has multiple blades attached on the disk and complex surface geometry. The refurbishment system will require further improvements involving a five-axis machine tool.

Further challenges remain in machining optimization. A typical blade consists of convex, concave faces and leading, trailing edges. Feed rate, scallop height, and step size control could be added to optimize the tool path. The overall time and surface finish could be further improved.

Other improvement is the complete automation of system. The system developed in this thesis requires human manipulation of probing and coordinate registration. A future extension of the current system could include programmed probing routine and software registration commands.

Appendix A

A.1 Simulated Blade Assembly

Dimensions in millimetres. Material: aluminum

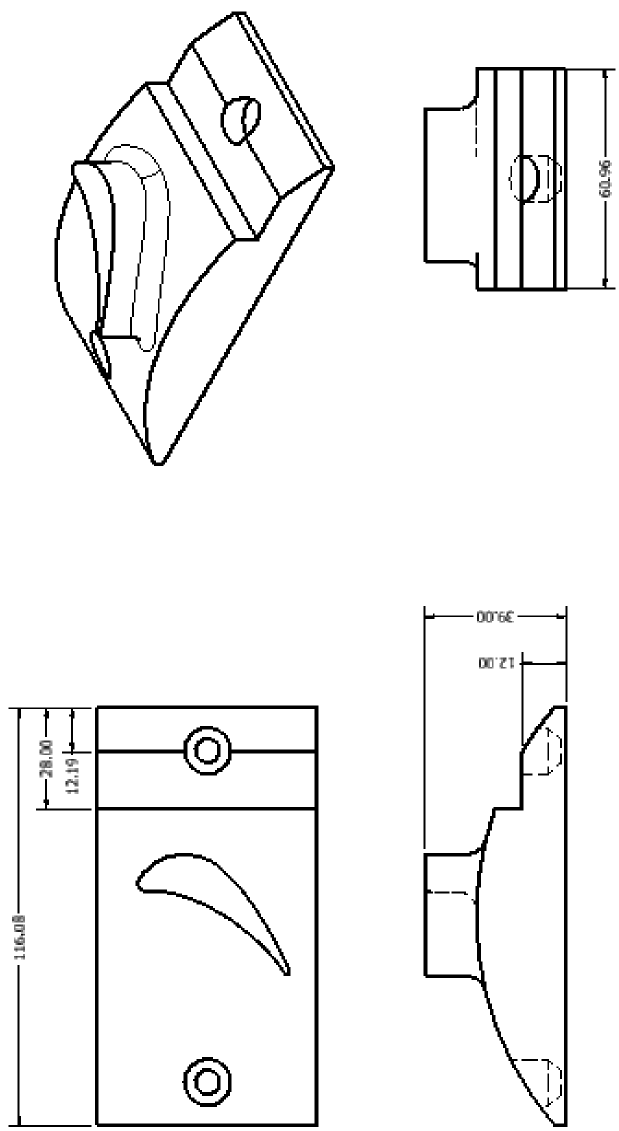

A.2 Fixture Disk

Dimensions in millimetres. Material: aluminum

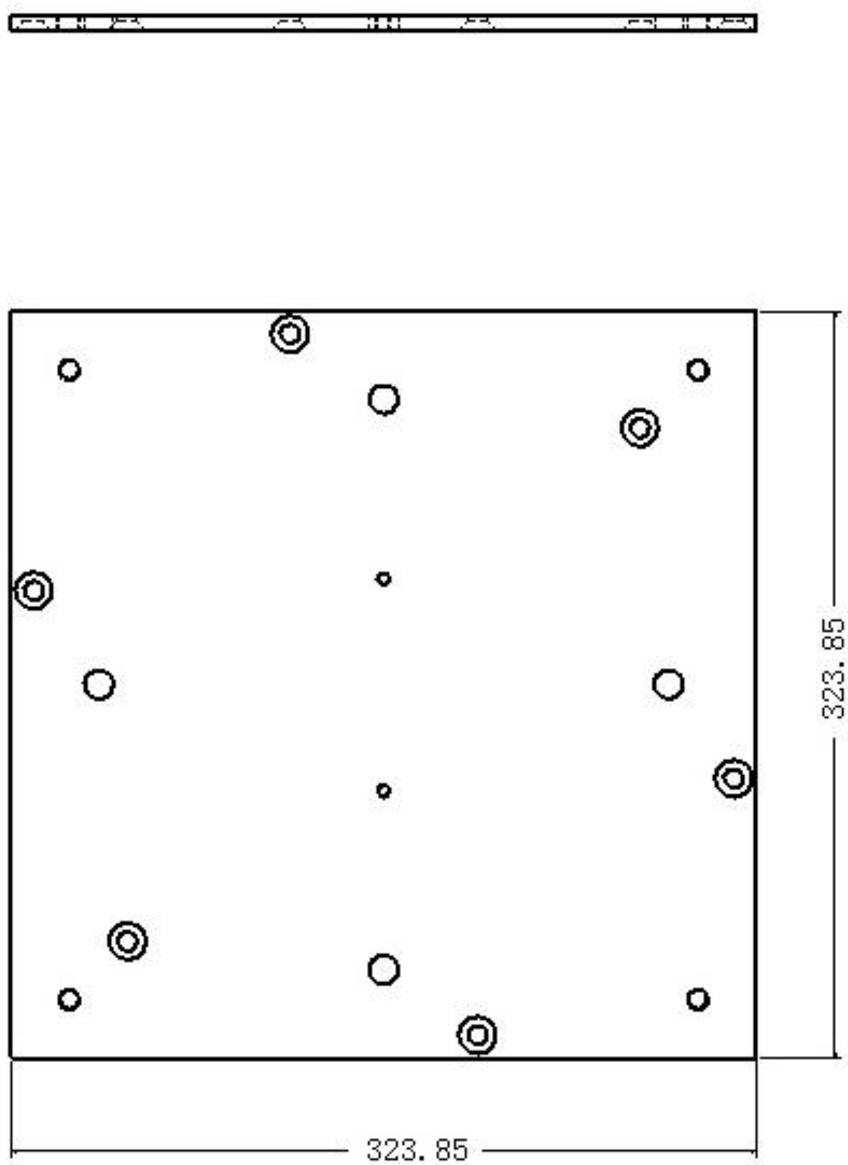

Appendix B

B.1 Nominal Tool Path Generation

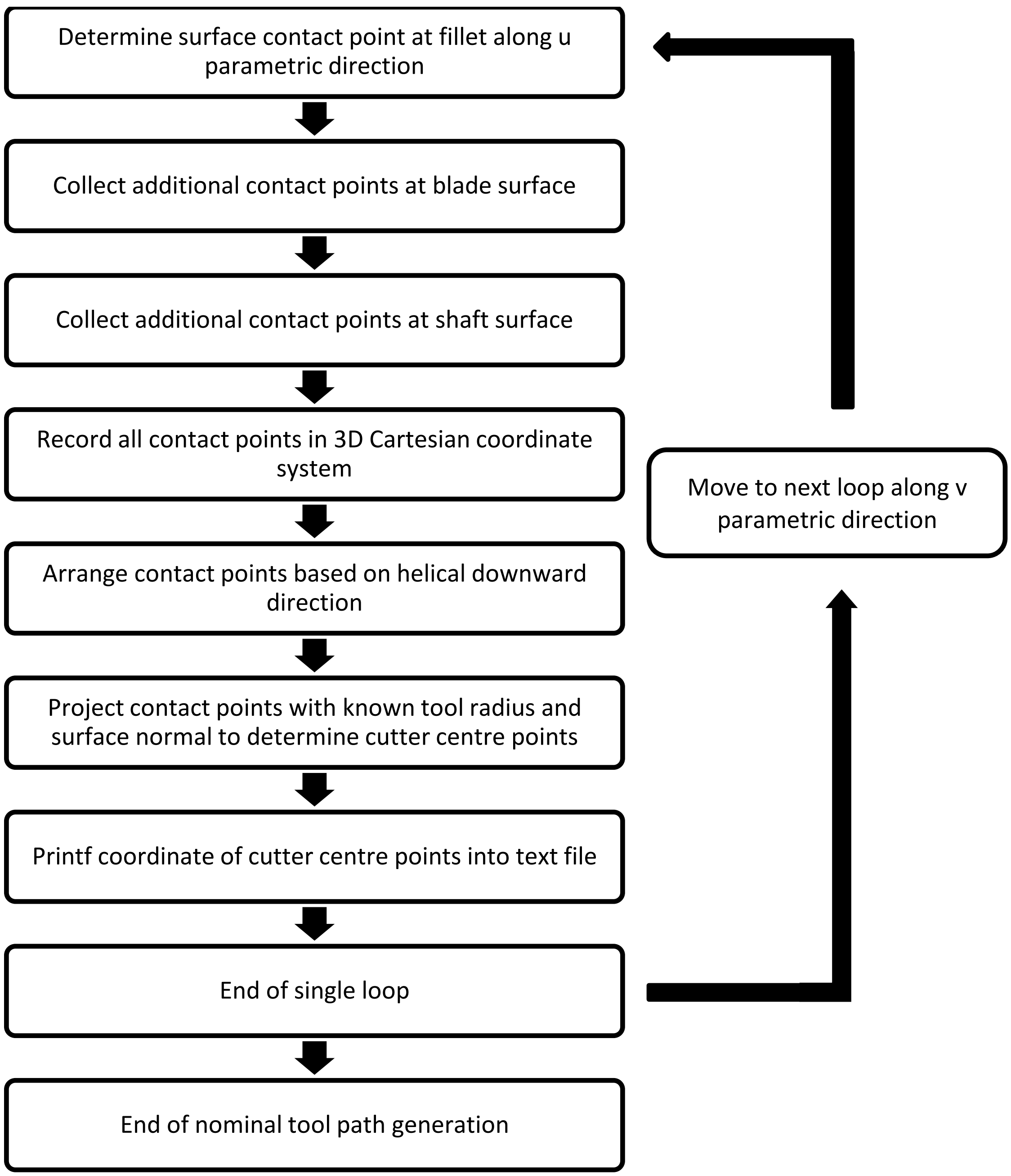

B.2 Customized Tool Path Generation

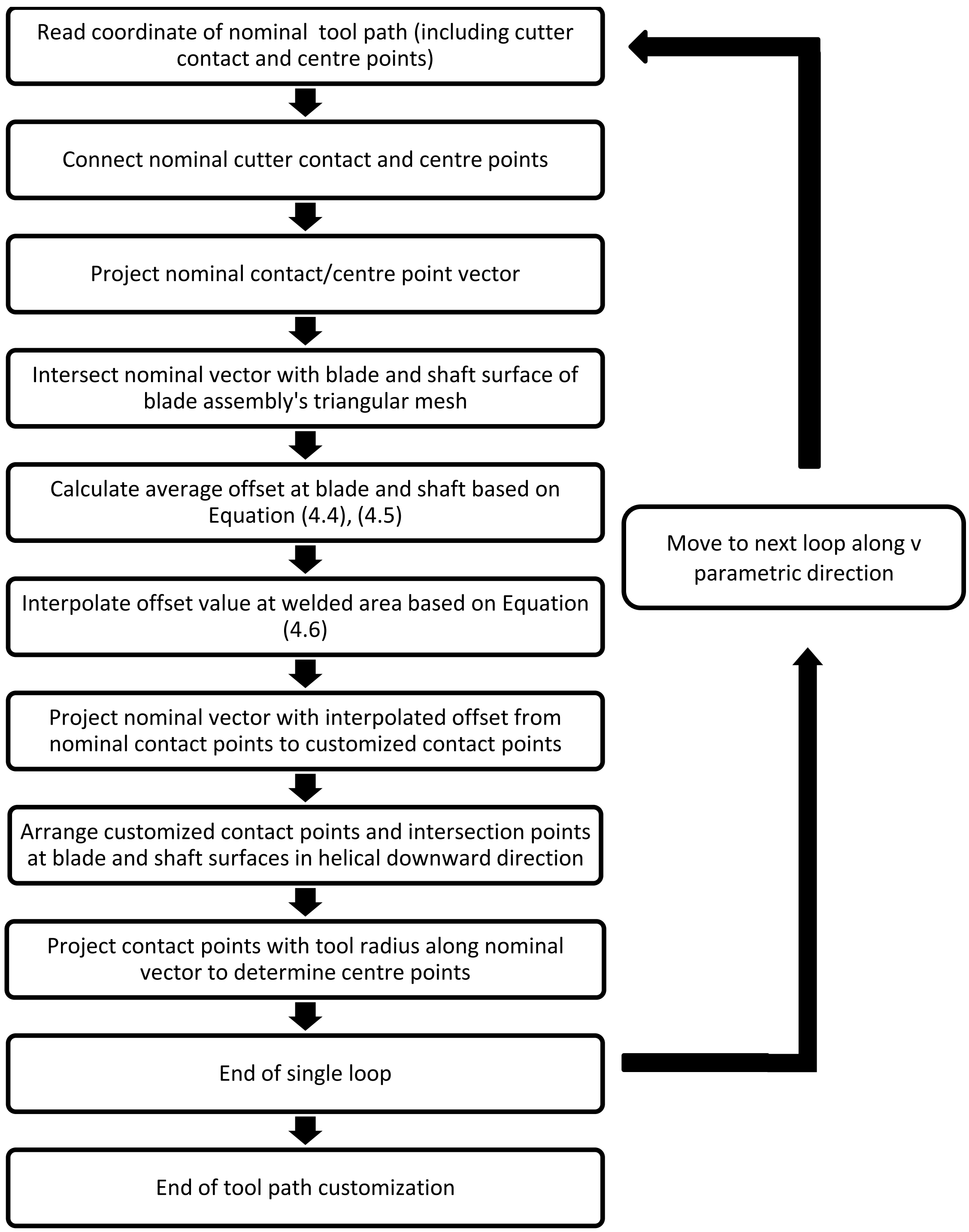

Reference

[1] D.A. Hills, "Mechanics of fretting fatigue," *Wear*, vol. 175, no. 1-2, pp. 107-113, 1994.

[2] Patrick J. Golden, "Development of a dovetail fretting fatigure fixture for turbine engine materials," *International Journal of Fatigue*, vol. 31, pp. 620-628, 2009.

[3] T. Nicholas, "Critical issues in high cycle fatigue," *International Journal of Fatigue*, vol. 21, pp. 221-231, 1999.

[4] Kazuhisa Miyoshi, Bradley A. Lerch, and Susan L. Draper, "Fretting wear of Ti-48Al-2Cr-2Nb," *Tribology International*, vol. 36, pp. 145-153, 2003.

[5] S.A. Meguid, P.S. Kanth, and A. Czekanski, "Finite element analysis of fir-tree region n turbine discs," *Finite Elements in Analysis and Design*, vol. 35, pp.

305-317, 2000.

[6] Antonio M. Mateo Garcia, "BLISK Fabricatin by Linear Friction Welding," in *Advances in Gas Turbine Technology*, Ernesto Benini, Ed.: InTech, 2011.

[7] Martin Bussmann and Erwin Bayer, "Market-oriented blisk manufacturing A challenge for production engineering," in *European Air and Space Conference*, 2007.

[8] Martin Bussmann, Jurgen Kraus, and Erwin Bayer, "An integrated cost-effective approach to blisk manufacturing," in *International Society for Air Breathing Engines*, 2005.

[9] H. Zhan, W. Zhao, and G. Wang, "Manufacturing turbine weight," *Aircraft Engineering and Aerospace Technology*, vol. 72, no. 3, pp. 247-251, 2000.

[10] Jian Gao, Janet Folkes, Oguzhan Yilmaz, and Nabil Gindy, "Investigation of a 3D non-contact measurement based blade repair integration system," *Aircraft Engineering and Aerospace Technology: An International Journal*, vol. 77, no. 1, pp. 34-41, 2005.

[11] R. V. Fleisig and A. D. Spence, "Intergrated Digitizing, Path Planning, and Five-Axis Machining for the Refurbishment of Compressor and Turbine Blades," *Manufacturing Science and Technology*, vol. 6, no. 1, pp. 31-38, 1997.

[12] G. Malone, "An integrated approach to remanufacturing turbine blades," *Welding Journal*, vol. 68, no. 6, pp. 20-26, 1989.

[13] Paul Walton, "Adaptive machining for turbine blade repair," *Modern Machine Shop*, vol. 80, no. 6, pp. 90-94, 2007.

[14] Paul Walton. (2002, April) Modern Power Systems. [Online]. http://www.modernpowersystems.com/story.asp?storyCode=2014616

[15] N.S. Ali, Reverse engineering of automotive parts applying laser scanning and structured light techniques, 2005.

[16] M. Nashman, T.H. Hong, W.G. Rippey, and M. Herman,., 1995.

[17] Renishaw plc. (2003) Renishaw resource centre. [Online]. http://resources.renishaw.com/details/MP12+Probe+System+data+sheet(71986

)(7859)

[18] F. Prieto, T. Redarce, R. Lapage, and P. Boulanger, "An automated inspection system," *International Journal OF Advanced Manufacturing Technology*, vol. 19, no. 12, pp. 917-925, 2002.

[19] Yadong Li and Peihua Gu, "Free-form surface inspection techiques state of the art review," *Computer-Aided Design*, vol. 36, pp. 1395-1417, 2004.

[20] Debbie Sniderman. (2010, Dec.) Desktop Engineer. [Online]. http://www.deskeng.com/articles/aaazje.htm

[21] K.H. Lee, H. Woo, and T. Suk, "Data reduction methods for reverse engineering," *International Journal of Advanced Manufacturing Technology*, vol. 17, no. 10, pp. 735-743, 2001.

[22] Roland DG Corp. (2012) Roland DG Corp. [Online]. http://www.rolanddg.com/product/3d/3d/lpx-re/specifications.html

[23] Wego Wang, *Reverse Engineering: Technology of Reinvention*.: CRC Press, 2010.

[24] K.L. Chui, W.K. Chiu, and K.M. Yu, "Direct 5-axis Tool-Path Generation from Point Cloud Input using 3D Biarc Fitting," *Robotics and Computer-Integrated Manufacturing*, pp. 270-286, 2008.

[25] Niloy J. Mitra, Natasha Gelfand, Helmut Pottmann, and Leonidas Guibas, "Registration of point cloud data from a geometric optimization perspective," *Eurographics Symposium on Geometry Processing*, pp. 22-31, 2004.

[26] H.T. Yau, "A model-based approach to form tolerance evaluation using non-uniform rational B-splines," *Robotics and Computer-Integrated Manufacturing* , vol. 15, no. 4, pp. 283-295, 1999.

[27] Ibrahim Zeid, *Mastering CAD/CAM*. New York: McGraw-Hill, 2005.

[28] G.T. Anthony and M.G. Cox, "Reliable Algorithms for Rougnness Assessment to BS3730," in *Software for Coordinate Measuring Machines*. Teddington, UK: National Physical Laboratory, 1986, pp. 30-37.

[29] I. Ainsworth, M. Ristic, and D. Brujic, "CAD-based measurement path planning for free-form shapes using contact probes," *International Journal of*

Advanced Manufacturing Technology, vol. 16, pp. 23-31, 2000.

[30] A.C. Lee, D.P. Chen, and C.L. Lin, "A CAD/CAM System from 3D Coordinate Measuring Machine," *International Journal of Production Research*, vol. 28, pp. 2353-2371, 1990.

[31] Shinju Kawabe, Fumihiko Kimura, and Toshio Sata, "Generation of NC commands for sculptured surface machining from 3-coordinate measuring data," *Annals of the CIRP*, vol. 29, no. 1, pp. 369-372, 1980.

[32] B.K. Choi, H.Y. Shin, Y.I. Yoon, and J.W. Lee, "Triangulation of scattered data in 3D space," *Computer-Aided Design*, vol. 20, no. 5, pp. 239-248, 1988.

[33] W. Sun, C. Bradley, Y.F. Zhang, and H.T. Loh, "Cloud data modelling employing a unified, non-redundant triangular mesh," *Computer-Aided Design*, vol. 33, pp. 183-193, 2001.

[34] Gregory C. Loney and Tulga M. Ozsoy, "NC machining of free form surfaces," *Computer-Aided Design*, vol. 19, no. 2, pp. 85-90, 1987.

[35] J.H. Cho, J.W. Kim, and K. Kim, "CNC Tool Path Planning for Multi-patch

Sculptured Surfaces," *International Journal of Production Research*, vol. 38, no. 7, pp. 1677-1687, 2000.

[36] Ali Lasemi, Deyi Xue, and Peihua Gu, "Recent Development in CNC Machining of Freeform Surfaces: A State-of-the-art Review," *Computer-Aided Design*, vol. 42, pp. 641-654, 2010.

[37] K. Suresh and C.H. Yang, "Constant scallop height machining of free-form surfaces," *Journal of Engineering for Industry, ASME Transaction*, vol. 116, no. 2, pp. 253-259, 1994.

[38] R.S. Lin and Y. Koren, "Efficient tool-path planning for machining free-form surfaces," *Journal of Engineering for Industry, ASME Transactions*, vol. 118, no. 1, pp. 20-28, 1996.

[39] Alan C. Lin and Hai-Terng Liu, "Automatic generation of NC cutter path from massive data points," *Computer-Aided Design*, vol. 30, no. 1, pp. 77-90, 1998.

[40] K.L Chui, K.M. Yu, and T.C. Lee, "Direct tool-path generation from massive point input," *Proceedings of Institution of Mechanical Engineers, Part B: Journal of Engineering Manufacture*, vol. 216, no. 2, pp. 199-206, 2002.

[41] Spatial Corp. (2012) Spatial Corp. [Online]. http://www.spatial.com/products/3d-acis-modeling

[42] Tech Soft 3D. (2012) Tech Soft 3D. [Online]. http://www.techsoft3d.com/

[43] Memex Automation Inc. (2012) Memex Automation Inc. [Online]. http://www.memex.ca/index.php?option=com_content&view=article&id=46&Itemid=200145

[44] Magnaflux. (2012) Magnaflux. [Online]. http://www.magnaflux.com/Products/PenetrantInspection/SpotcheckVisible/Developers/SKDS2.aspx

[45] Rejean Baribeau and Marc Rioux, "Influence of speckle on laser range finders," *Applied Optics*, vol. 30, no. 20, pp. 2873-2878, 1991.

[46] Seokbae Son, Huunpung Park, and K.H. Lee, "Automated laser scanning system for reverse engineering and inspection," *International Journal of Machine Tools and Manufacture*, vol. 42, pp. 889-897, 2002.

[47] H.Y. Feng, Yixin Liu, and Fengfeng Xi, "Analysis of digitizing errors of a laser scanning system," *Journal of the International Societies for Precision Engineering and Nanotechnology*, vol. 25, pp. 185-191, 2001.

[48] Tahir Rabbani, Sander Dijikman, Frank van den Heuvel, and George Vosselman, "An Integrated Approach for Modelling and Global Registration of Point Clouds," *ISPRS Journal of Phtogrammetry and Remote Sensing*, vol. 61, no. 6, pp. 355-370, 2007.

[49] Geomagic. (2012) Geomagic. [Online]. http://www.geomagic.com/en/products/qualify/overview/

[50] Magnaflux. (2012) Magnaflux Spotcheck SKD-S2 Non-aqueous Developer. [Online]. http://www.magnaflux.com/DesktopModules/Bring2mind/DMX/Download.aspx?Command=Core_Download&EntryId=12681&PortalId=0&TabId=396

[51] Roger Cortesi. Tool Deflection Calculation. [Online]. http://rogercortesi.com/portf/minimill/tool_stiffness/sld004.htm

[52] F. Abrari, M. A. Elbestawi, and A. D. Spence, "On the dynamics of ball end

milling: modeling of cutting forces and stability analysis," *International Journal of Machine Tools and Manufacture*, vol. 38, no. 3, pp. 215-237, Feb. 1998.

[53] George Tlusty, "Forces and Forced Vibrations in Milling," in *Manufacturing Process and Equipment*.: Prentice Hall, 1999, pp. 537-578.

[54] (2012) Brown & Sharpe. [Online]. http://www.brownandsharpe.com/applications/intro-to-coordinate-metrology/the-part-coordinate-system

[55] C.H. Menq, H.T. Yau, and G.Y. Lai, "Automated precision measurement of surface profile in CAD-directed inspection," *IEEE Transactions on Robotics and Automation*, vol. 8, no. 2, pp. 268-278, 1992.

[56] Rolls-Royce. (2003, Apr.) F-16.net. [Online]. http://www.f-16.net/f-16_forum_viewtopic-t-9880-start-30.html